Utilizing Machine Learning Techniques to Identify Autism Spectrum Disorder Using fMRI Data

By

Jansen Long

A thesis submitted in partial fulfillment

of the requirements for the degree of

MASTER OF SCIENCE

in

Computer Science

Middle Tennessee State University

December 2023

Thesis Committee:

Dr. Xin Yang

Dr. Joshua Philips

Dr. Arpan Sainju

ACKNOWLEDGEMENTS

I would like to express my thanks to my advisor for this project, Dr. Xin Yang, for her guidance in researching this topic. I would also like to thank Dr. Joshua Phillips and Dr. Arpan Sainju for taking the time to serve on this thesis committee. I am also grateful to all my friends and family for supporting me throughout this process. I truly could not have done this without all of your support.

ABSTRACT

This study extensively investigates Autism Spectrum Disorder (ASD) classification by analyzing functional connectivity derived from functional magnetic resonance imaging (fMRI) data. ASD is a neurological development disorder affecting 1 in 36 US children, underscoring the importance of early detection for effective intervention. Using Autism Brain Imaging Data Exchange (ABIDE) fMRI data, this research evaluates the predictive capabilities of the Automated Anatomical Labeling (AAL), cc200, and cc400 brain atlases. Functional connectivity is assessed through correlation, covariance, tangent, partial correlation, and precision measures. Support Vector Machines (SVMs) and a proposed Convolutional Neural Network (CNN) are employed for classifying ASD, with the CNN achieving comparable results: 68.11% accuracy, 73.45% AUC, 73.41% recall, and 69.27% precision. Notably, correlation, tangent, and covariance measures show robust performance across the assessed brain atlases. This research provides valuable contributions by thoroughly comparing various functional connectivity analyses for ASD classification, shedding new light on their comparative effectiveness.

TABLE OF CONTENTS

LIST OF TABLES

LIST OF FIGURES

CHAPTER I.

INTRODUCTION

Autism Spectrum Disorder (ASD) is a neurological developmental disorder, that affects individuals in diverse ways, creating difficulties in social interactions, communication, and the occurrence of repetitive behaviors. According to the Centers for Disease Control and Prevention (CDC), approximately 1 in 36 children in the United States have been diagnosed with ASD as of 2020, which is considered a pervasive developmental disorder [3]. As shown in Figure 1, cases of ASD have been on the rise in recent years [4]. Symptoms of ASD

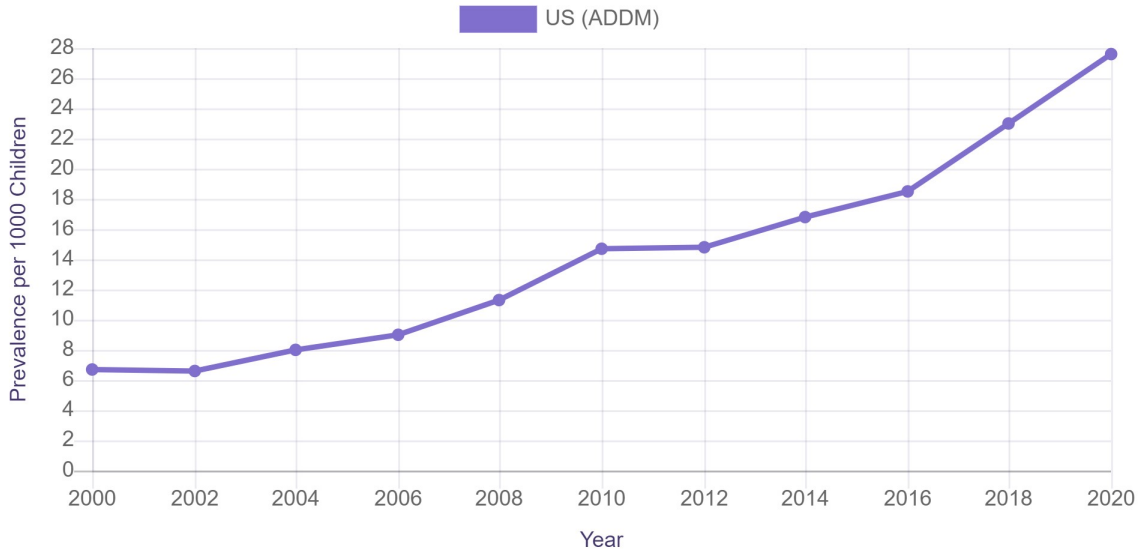

Figure 1: An estimate of the prevalence of ASD per 1000 children in the United States as per the Center for Disease Control [2]

include difficulty communicating, repetitive behaviors, and restricted interests. People with ASD may also have different ways of learning, moving, and paying attention. This can make behaviors that are considered common to the general public more difficult and can often make interacting with others more challenging. As children with ASD mature, they often have difficulties developing and maintaining relationships as well as understanding social cues and expectations in both educational and professional environments [2]. Diagnosing neurological disorders can be a challenge, as it often requires medical professionals to

monitor the behaviors of a patient in order to establish a diagnosis and a subsequent treatment plan [2]. In order to be diagnosed with ASD, an individual must present symptoms as defined by the fifth edition of the Diagnostic and Statistical Manual of Mental Disorders (DSM-5) – which is central to diagnosing mental and behavioral disorders [1, 5]. The deficits associated with an ASD diagnosis as given by the DSM-5 are given in Table 1. Treatment for this disorder seeks to cater toward the individual in an effort to minimize the effect of symptoms on the individual's quality of life. Treatment is most effective early in a child's life; therefore, most screening is done with respect to normal development patterns and milestones in young children. It is important to diagnose ASD early so that treatment can begin at a young age, thus minimizing symptoms later in life.

Traditionally, diagnosis requires the observation of behaviors that are typical of ASD patients over a period of time [2]. Screening children for ASD has typically involved reporting abnormal behavior to a primary care provider, who would then administer an initial screening test to determine whether or not a child has a high likelihood of suffering from ASD [6]. If it is determined that a child has a high likelihood of suffering from ASD, they will be referred to a second level of screening. If the second screening process also determines that a child may have ASD, they are then referred to a specialist for a final evaluation for ASD. These tests include parental questionnaires, interviews, or evaluation of interactions with the primary care provider. While these tests are capable of detecting warning signs of ASD, they have several drawbacks as a primary way of diagnosing the condition. They can suffer from biases from a parent, caretaker, or primary care provider. They also have intrinsic limitations in that many of the abnormal behaviors that are characteristic of ASD could be considered 'normal' behaviors of children still in infancy. They only become 'abnormal' when they last longer in the child's life than is expected. This forces there to be a minimum age at which these tests have the capacity to accurately assess a child's development. This makes it more difficult to diagnose ASD as

Table 1: The diagnostic criteria for Autism Spectrum Disorder as given by the DSM-5 [1].

Deficit Categories	Deficits
1. Persistent deficits in social communication and social interaction across multiple contexts, as manifested by the following, currently or by history; must have all 3 symptoms in this domain	• Social-emotional reciprocity • Nonverbal communicative behaviors used for social interaction • Developing, maintaining and understanding relationships
2. Restricted, repetitive patterns of behavior, interests, or activities, as manifested by at least 2 of the following, currently or by history; must have 2 of the 4 symptoms	• Stereotyped or repetitive motor movements, use of objects, or speech • Insistence on sameness, inflexible adherence to routines, or ritualized patterns or verbal nonverbal behavior • Highly restricted, fixated interests that are abnormal in intensity or focus • Hyper- or hyporeactivity to sensory input or unusual interests in sensory aspects of the environment

early as possible. Additionally, the reliance on longitudinal testing can lead to difficulty in diagnosing ASD reliably and efficiently at young ages. The younger a person is diagnosed with ASD, the more effective treatment can be at lessening symptoms.

The American Academy of Pediatrics recommends that testing be done universally between 18 to 24 months of age. However, there is concern in the medical community that this may be harmful, as medical professionals are wary of misdiagnosing via universal screening. The concern over universal ASD screening has to do with the low prevalence

of ASD in the population – roughly 2% of children are diagnosed with the condition. As explained in the study done by McCarty et. al, current screening tools are still likely to incorrectly refer a significant portion of children for further evaluation [6]. This places undue stress on the families of children being screened and the medical providers needing to conduct more patient screenings.

These factors lead to the need for multiple modes of performing reliable testing for ASD. According to McCarty et. al, screening for ASD should be a multi-step process in order to confirm the validity of the referral so as to not put a strain on the resources of specialists in ASD evaluation [6]. The more patients incorrectly referred to these specialists, the longer it may take for patients who were correctly identified to receive treatment. McCarty suggests that developing effective biomarker tests as a part of this process would help relieve concerns that care providers have about screening children for ASD. This would be done in conjunction with tests proposed by the American Academy of Pediatrics to do the following: identify which children are at risk and therefore should be screened, used as a secondary screen, and/or confirm behavioral observations. The development of an effective biomarker test for ASD would help to efficiently and quickly diagnose the condition thus improving the age at which children are able to be diagnosed. This would mean that children would be able to be diagnosed at younger ages and begin the therapeutic interventions that have been shown to lessen the severity of symptoms.

This urgency has prompted researchers to investigate tools that leverage biomarkers, among which functional Magnetic Resonance Imaging (fMRI) has emerged as a valuable tool for detecting potential biomarkers in expedited and refined diagnostic procedures. As ASD is a neurological development disorder, many researchers are interested in using neuro-imaging techniques as a potential step in the diagnostic process. Functional Magnetic Resonance Imaging (fMRI) is a mode of neuro-imaging that creates an image of the brain by measuring the Blood Oxygenation Level Dependent (BOLD) contrast in the subject's brain

over a period of time. When hemoglobin is carrying oxygen to cells it is diamagnetic which is indistinguishable from brain tissue. However, once neurons have used the oxygen carried by the hemoglobin, the hemoglobin becomes paramagnetic which is distinguishable from brain tissue. This change in oxygen level allows for the ability to measure brain activity over the course of time as there is a strong correlation between neural activity and the deoxygenation of blood [7]. This makes fMRIs an effective tool in diagnosing neurological issues – such

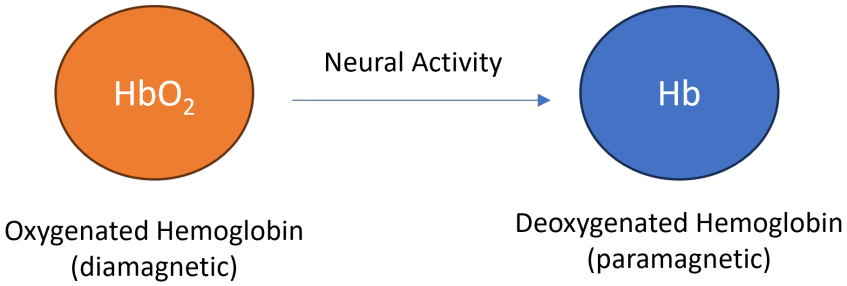

Figure 2: A diagram showing the BOLD contrast measure.

as Schizophrenia, Attention Deficit Hyperactivity Disorder (ADHD), Alzheimer's disease, and ASD – as it is able to provide measurements for an individual's brain functions, without requiring invasive procedures or injections to accurately visualize the brain [8, 9, 10, 11].

With the significant role of fMRI in neuroimaging research, there has been a growing focus on functional connectivity measures in recent years. The popularity of functional connectivity lies in its ability to uncover complex patterns of brain activity and interactions. Notably, the use of functional connectivity measures in machine learning analysis has gained widespread popularity. This approach enables a more thorough understanding of the intricate relationships between brain regions, providing valuable insights into neural networks and their implications across various cognitive processes. The purpose of these measures is to summarize the correlation between activity in one region of the brain with other regions of the brain. A study by Ju et. al has shown functional connectivity measures to be more sensitive to disease than fMRI time series data [12]. The most prevalent functional connectivity measure used for fMRI classification is Pearson correlation [13, 11, 14, 15, 16, 17]. Nevertheless,

alternative approaches for representing functional connectivity measures in fMRI, not extensively documented in existing literature, warrant thorough investigation. It is imperative to systematically compare these distinct functional connectivity measures to discern their predictive capability in the classification of ASD.

This project focuses on classifying ASD by training artificially intelligent models on fMRI data obtained from the Autism Brain Imaging Data Exchange (ABIDE) data repository [18]. The ABIDE repository is a publicly available data set that has been used in many studies [18, 11, 16, 19]. It has shown great promise as there have been accuracies as high as 75% on the full data set, but when reduced to only viewing each site individually, accuracy increases to as high as 80% at the cost of reducing the overall generality of the model [11]. While these performances show promise, there is still room for improvement in these classification models. Innovations are still essential for refining these models to be acknowledged as effective tools for detecting ASD.

The primary objective of this study is to comprehensively investigate the ASD classification through an in-depth analysis of functional connectivity derived from fMRI data. Utilizing fMRI data obtained from the ABIDE repository, the performance of the Automated Anatomical Labeling (AAL), cc200, and cc400 brain atlases is evaluated for their predictive capability in relation to ASD classification. The investigation into functional connectivity involves assessing various measures, including correlation, covariance, tangent, partial correlation, and precision. Support Vector Machines (SVMs) and a proposed simple Convolutional Neural Network (CNN) are employed to accomplish these tasks. The proposed Convolutional Neural Network (CNN) model achieves comparable performance metrics, including an accuracy of 68.11%, an Area Under the Curve (AUC) of 73.45%, a recall of 73.41%, and a precision of 69.27%. Additionally, it is noteworthy that correlation, tangent, and covariance connectivity measures exhibit robust performance across the assessed brain atlases. In conclusion, this research offers a valuable contribution to the field by conducting

a thorough investigation into the ASD classification through various functional connectivity analyses, which have not been thoroughly compared before.

CHAPTER II.

BACKGROUND

Data Background

In this study, the dataset was obtained from the Autism Brain Imaging Data Exchange (ABIDE) [18], comprising 1112 fMRI images (539 ASD patients and 573 control subjects) along with corresponding phenotypic data for each patient. This dataset comes from sixteen sites across the world. Preprocessing for fMRI data plays a crucial role in ensuring the quality and reliability of subsequent analyses, such as functional connectivity, activation mapping, and machine learning applications. The data is retrieved using the nilearn Python library for neuro-imaging data [20]. Using nilearn, the Configurable Pipeline for the Analysis of Connectomes (CPAC) preprocessed version of the quality checked dataset was used [21]. CPAC is a configurable, open-source processing pipeline that was created to automatically and reliably process large amounts of fMRI data. The CPAC preprocessing method has been shown to perform best for ASD detection of all preprocessing methods [16]. The preprocessing performed by CPAC includes motion correction, anatomical/functional coregistration, spatial normalization, spatial and temporal filtering, tissue segmentation, slice-timing correction, several variations of nuisance signal removal (such as increased heart rate or respiration), and volume censoring (motion "scrubbing"). CPAC along with quality checking, reduces the dataset to 871 subjects with 403 patients with ASD and 468 control patients.

fMRI data is commonly partitioned into different regions of interest (ROIs). Once the brain has been split into these regions, the full map of the brain is called an atlas, as shown in figure 3. Traditionally, atlases such as Automated Anatomical Labeling (AAL) separate regions based on the physical anatomy of the brain and have been used for fMRI analysis [22, 23, 10, 24, 25]. However, dividing the brain this way provides less information about the connectivity of neurons as compared to other methods [26]. To overcome this limitation,

researchers have introduced innovative connectome-based approaches. The cc200 and cc400 atlases represent sophisticated connectome-based approaches to brain parcellation. Unlike traditional anatomically driven atlases, these connectome-based schemes are designed with a specific emphasis on the functional interactions and connectivity patterns between different brain regions. For the experiments detailed in this project, three commonly used atlases were tested: AAL, cc200, and cc400. The AAL atlas segments the brain into 116 ROIs, the cc200 atlas segments the brain into 200 ROIs, and the cc400 atlas segments the brain into 392 ROIs.

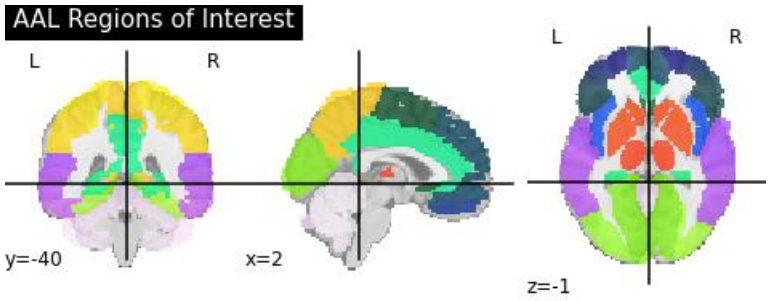

Figure 3: AAL Regions of interest shown using the Python module nilearn.

Functional Connectivity Measures

An fMRI image is a 4-dimensional data structure, a 3-dimensional image over a period of time. It is common to use functional connectivity measures to transform this data structure so that it can be easily visualized and utilized by common machine learning algorithms. Additionally, it has been shown that functional connectivity measures are more sensitive for disease classification than time series methods in a study by Ju et. al [12]. The purpose of functional connectivity is to calculate the correlation between the level of activity in one region of interest with the level of activity in other regions of interest. This changes the representation of an fMRI image from a 4-dimensional image to an N x N matrix, where N is the number of ROIs in the atlas.

The most commonly used functional connectivity measure is Pearson Correlation which is used predominantly in the literature [11, 16, 27, 13, 17]. However, there are other

functional connectivity measures that are utilized less frequently. In addition to Pearson correlation, this study utilizes the covariance measure, partial correlation, tangent measure, and precision measure as functional connectivity measures for this dataset. In the literature, these connectivity measures have not been compared in depth for their ability to classify fMRIs as ASD positive or negative.

Functional Connectivity is found by first calculating the empirical covariance matrix, C, for each subject [28]. Covariance in the context of fMRIs is a measure of the relationship between each ROI over all time steps. The Ledoit-Wolf estimator for covariance is used in this study [29]. This creates an N x N matrix, where N represents the number of ROIs and each value, x, can be represented by $-\infty \leq x \leq +\infty$.

All functional connectivity measures used in this study can be written in terms of a covariance matrix C. Pearson Correlation is applied to the covariance matrix as shown in the formula below [15].

$$Correlation = \frac{cov(X,Y)}{\sigma_X * \sigma_Y}$$

Where σ is the standard deviation of regions of interest, X and Y. The Precision measure is found by taking the inverse of C using Cholesky decomposition [30]. The Partial Correlation matrix, ρ, is defined as the standardization of $-C^{-1}$.

The tangent functional connectivity takes the covariance matrix and maps it to a tangent space [31]. This is done using the equation below.

$$\vec{C} = \log_m (C_G^{-\frac{1}{2}} * C * C_G^{-\frac{1}{2}})$$

Where C_G represents an average of all covariance matrices in a population and $\log_m$ is a matrix logarithm. This is done so that all covariance matrices are projected to the same tangent plane.

Support Vector Machine (SVM) Background

SVMs for Classification

A Support Vector Machine (SVM) is an algorithm that is commonly used in classification tasks with a large amount of success [32]. SVMs attempt to find a hyperplane which separates the classes for which the distance to the nearest data point of both classes is maximized and greater than the bias. The bias is decided before training. The hyperplane can be described by the following formula.

$$\vec{w} * \vec{x} + b = 0$$

Where $\vec{w}$ is an n-dimension weight vector, $\vec{x}$ is an input vector, and b is the bias specified in the algorithm. The algorithm computes the distance between vectors and the hyperplane using the following formula for all data items; however, the only distances that the algorithm is maximizing are the closest vectors to the hyperplane for each potential class as shown in the expression below. These are the support vectors from which the algorithm gets its name.

$$d = \frac{|\vec{w} * \vec{x_i} + b|}{||\vec{w}||}$$

This creates an optimization problem where you are trying to find the maximum distance, d, between the hyperplane and the support vector for each class. This problem involves finding the weights of the optimal hyperplane given a regularization parameter, C, that allows for misclassification in order to avoid overfitting to the training data.

This algorithm is very useful for classifying data, but it only works for linearly separable cases as shown above. In order to separate data items that may not be linearly separable, researchers use the kernel trick to expand data into a higher dimensional space and classify data in that higher dimensional space [32]. This allows the use of the same optimization

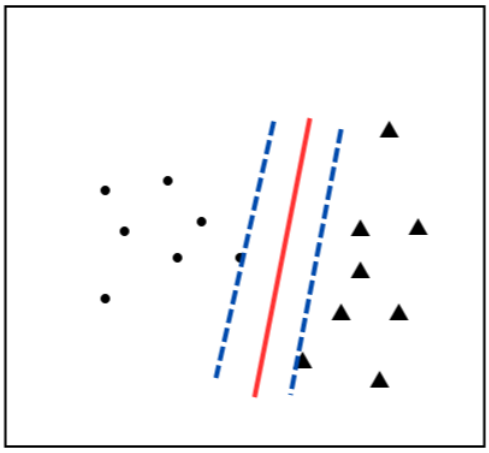

Figure 4: A simplified example of an SVM problem. The red line represents the decision boundary, the data point nearest to the decision boundary is a support vector, and the blue lines represent the margin allowed between the support vector and the decision boundary.

problem as above and allows for non-linear separation of classes by implicitly mapping the data to a higher dimensionality. This is done with the help of a kernel function. Popular kernel functions are as follows: Linear Kernel, Polynomial Kernel, Radial Basis Function (RBF) Kernel, and Sigmoid Kernel [33]. There is no one kernel that is best in all cases, so in problems with high dimensional data, it can be difficult to intuit which kernel best fits the shape of the data. Therefore, researchers must test different kernels to determine which kernel best fits their domain [32].

SVMs for fMRI Classification

SVMs are a versatile tool for classification. They have been used for fMRI classification in several different neurological disorder detection problems such as ASD [34], Schizophrenia [8], Alzheimer's [35]. They have also been used as non-diagnostic tools such as object detection classification [36], where the model was trained to predict what image a subject was being shown during an fMRI. SVMs are among the most popular algorithms to use for these problems due to fast training times with a high success rate. For example, S. Hojjati et

al. reported an accuracy of 91.4% in predicting when cases of Mild Cognitive Impairment will convert to Alzheimer's disease over time and achieved a 92.1% accuracy in detecting Schizophrenia in the study's subjects [8, 9]. These performances show great promise in utilizing SVMs to classify fMRI data modality.

There is precedent for using SVMs to detect ASD using fMRI data. Eslami et al. report an accuracy of 72% when using SVMs for ASD classification and 80% for a model utilizing both SVMs and deep neural networks for classification of ASD subjects [11]. An accuracy of 80% is the most effective model to date for ASD classification on the ABIDE dataset; however, the experiments were performed on subsections of the ABIDE dataset where the models were only trained using data from particular sites instead of a cross-section whole dataset. This experiment also did not focus on testing different functional connectivity measures for transforming the data into a vector space. SVMs are also commonly used as a control model for comparison [11, 14, 13, 19].

Convolutional Neural Network (CNN) Background

Convolutional Neural Networks Theoretical Basis

Convolutional Neural Networks (CNNs) are a type of feed-forward neural network architecture that is based upon sight receptors [37]. CNNs involve a convolutional layer in which an n x n matrix is given as input and a smaller kernel is defined. That kernel is then moved along the input matrix and an activation function is applied to the inputs of a group of inputs to determine what value should be passed to the next layer. For each $k \times k$ group of input values, there are a specified number of outputs called filters. This process is visualized in Figure 5 below. It is common to pass values from a Convolutional layer to a pooling layer, in which the filters are then down-sampled and passed to the next layer of neurons. Common pooling techniques are taking the maximum or the average of the values filtered through the convolutional layer. CNNs were proposed to help to improve image recognition. They are particularly useful because they are able to group together parts of the input that

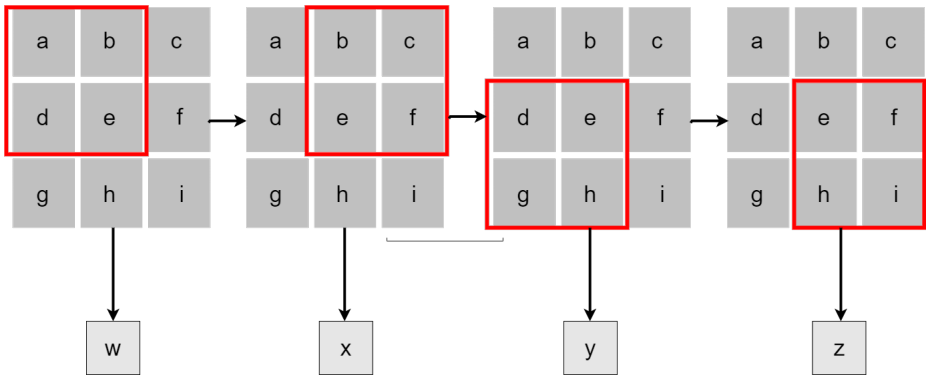

Figure 5: An example convolution with a 3 x 3 input, a 2 x 2 kernel where w, x, y, and z represent the output of each grouping of input values respectively.

are spatially close to each other. This can be done because regions of an image that are near to each other are likely to be related to one another. This improves object recognition for images as well as reduces space complexity that is involved in using a fully connected artificial neural network for similar tasks [37].

Convolutional Neural Networks for Functional Connectivity Data

Convolutional Neural Networks are typically applied to computer vision problems, however, there have been some attempts to apply this technique to graphical data [38]. There have been several attempts to use CNNs to classify ASD using fMRI data [14, 17, 13].

The highest accuracy reported when using Convolutional Neural Networks to classify ASD using fMRI data was reported by Khosla et. al with a reported accuracy of 73.1% and an AUC score of 75.8% [13]. For that study, an ensemble 3D-CNN model was used, which utilized multiple instances of a 3D-CNN model across a wide range of atlases. The fMRI data was transformed into functional connectivity matrices using the Pearson correlation functional connectivity measure. Each input channel for the 3D-CNN model represents a voxel level "connectivity fingerprint". A "connectivity fingerprint" is a mapping of the connectivity values for an ROI onto the gray matter mask which the given atlas was derived from, creating a 2-dimensional image. This image is created for all regions and given as

input to the model such that there are N images –one for each channel where N is the number of ROIs in the atlas being used. This input is fed into 4 convolutional layers in sequence using several down-sampling techniques such as average pooling and max pooling. The output of those convolutional layers is flattened and given as input to a dense layer with 32 units which is connected to a sigmoid output unit. The details of the model are given in Figure 6. This model was trained and tested on the Harvard-Oxford, cc200, Eickhoff-Zilles, Talaraich and Tournox, Dosenbach 160, AAL and cc400 atlases. The highest accuracy achieved using an individual atlas is 71.7% using the cc400 atlas. When used as an ensemble classifier using models trained on each individual atlas, the accuracy improves to 73.1%. The number of parameters for this model was not reported.

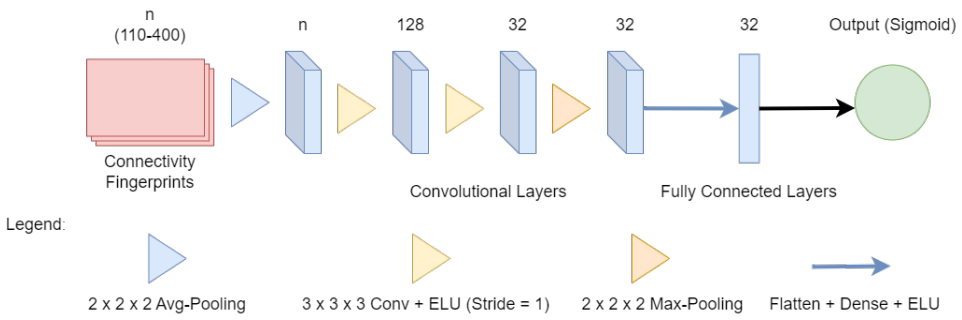

Figure 6: A plot of the architecture as defined by Khosla et. al. The number of channels is defined above.

The model proposed by Sherkatghanad et. al achieved a reported 70.22% accuracy. This model uses the Pearson correlation functional connectivity measure on the cc400 atlas. The Pearson correlation functional connectivity measure is fed into 7 parallel convolutional layers with kernel sizes ranging from 1×392 to 7×392. The filter sizes of each convolutional layer are from values 392×400 to 386×400. The output size of each convolutional layer is reduced to 1×400 using a max pooling layer and then concatenated into one vector of size 1×2800. During training, only 25% of these pooled weights are kept to minimize overfitting. The resulting values are fed into a fully connected layer and then into a softmax output layer. This creates a model with 4,398,802 parameters. A plot of this model is shown

in Figure 7.

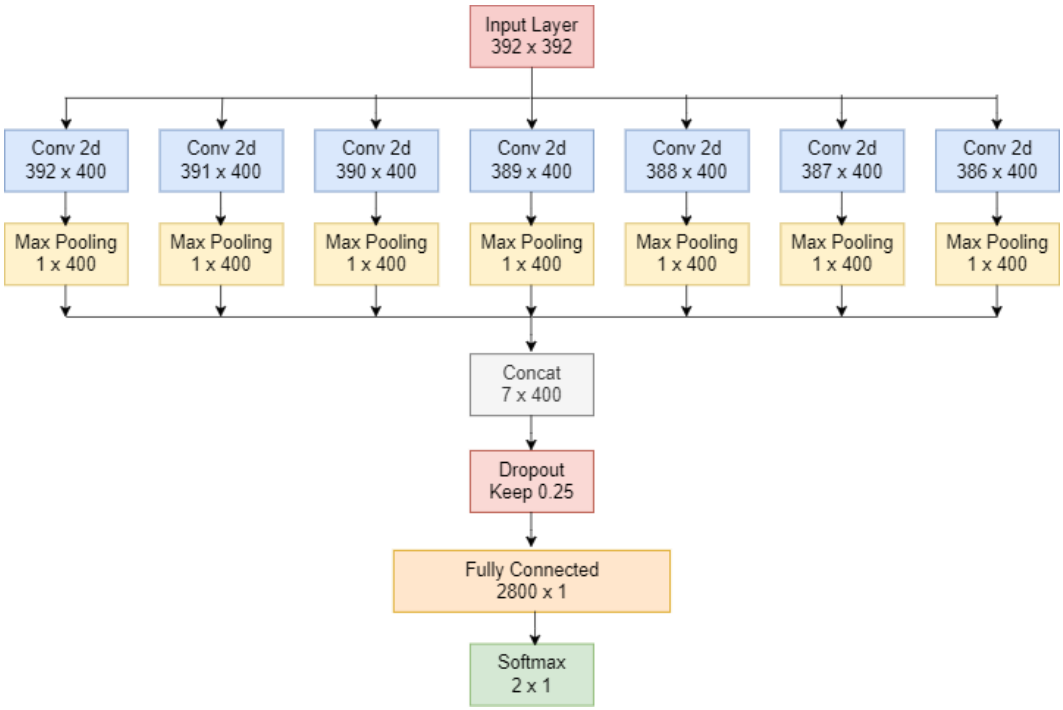

Figure 7: A plot of the CNN architecture as defined by Sherkatghanad et. al.

In the study conducted by Xing et. al, an accuracy of 66.88% was reported [17]. In that study, the Pearson correlation functional connectivity matrix was input to an "Edge to Node with Element Wise Filters" (E2N-EW) layer. This layer does not have weight sharing between elements like a typical CNN. This outputs a matrix of size $N \times N$ – where N is the number of regions of interest – into a Convolutional layer with a kernel size of $1 \times N$ where N is the number of regions of interest. This second layer outputs N filters into a fully connected layer which is then fed into a softmax layer for output. The AAL atlas was used for the experiments conducted by Xing et. al; therefore, N is 116. This creates a model with 1,268,160 parameters. A plot of this model is shown in Figure 8.

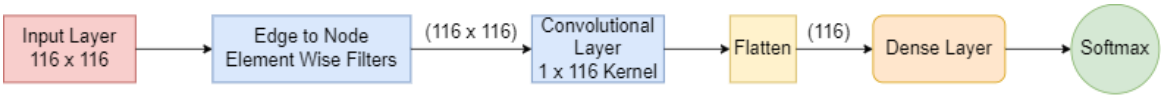

Figure 8: A plot of the CNN architecture as defined by Xing et. al.

Despite the success of CNN models, additional functional connectivity measures other than Pearson correlation have not been explored or compared for any CNN architecture in the literature to date.

CHAPTER III.

METHODOLOGY

In this study, a simple Convolutional Neural Networks (CNN) and Support Vector Machines (SVMs) are used to classify fMRI data as ASD positive or ASD negative. In order to effectively use these algorithms, the raw fMRIs were converted to functional connectivity matrices using different connectivity measures. Connectivity Matrices are calculated using the Python module Nilearn, which has built-in methods for importing, utilizing, and transforming fMRI data. This study tests the following connectivity measures: Pearson Correlation, Covariance, Precision, Tangent, and Partial Correlation as they are implemented in the nilearn neuro-imaging python package [20]. These connectivity measures underwent testing using three distinct brain atlases: AAL, cc200, and cc400. Because these atlases identify different regions of interest, computing the functional connectivity will result in matrices that are represented differently despite being derived from the same subject. An overview of the study is shown in Figure 9.

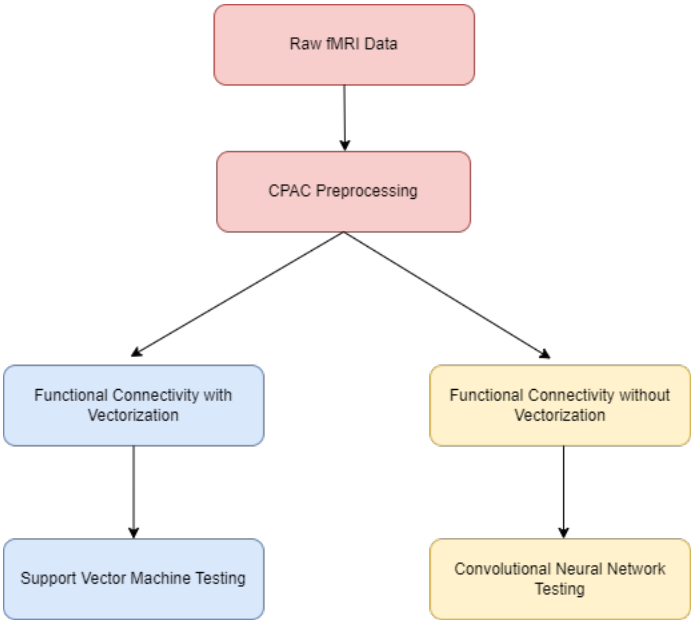

Figure 9: An overview of the flow of the study.

Data Preparation

The data was retrieved from the ABIDE repository, which includes 1112 fMRI images – 539 ASD patients and 573 control subjects – which is trimmed down to 871 using the CPAC preprocessing pipeline and quality checking as given by the nilearn python library. For the CNN model, the labels are one-hot encoded. Once each class is properly represented, each fMRI image is converted into its corresponding functional connectivity values. For SVMs, the functional connectivity matrix is represented as a vector. In vectorizing the matrix, the matrix is halved along the diagonal to remove duplicate values. For CNNs, the algorithm requires a 2-dimensional kernel to move along the matrix to select a number of filtered values; therefore, the entire functional connectivity matrix is used, as the 2-dimensional representation is needed.

Experiment Design

Each algorithm underwent testing through repeated 10-fold cross-validation, with the data shuffled for each iteration, and the validation process was reiterated 5 times. The metrics that were collected include accuracy, area under the curve (AUC), recall, and precision. Each algorithm was tested using all combinations of Functional Connectivity Measures and atlas as mentioned above.

For each combination of Atlas and Functional Connectivity Measure, Support Vector Machines were tested using the following kernels: Linear, Radial Basis Function (RBF), Polynomial, and Sigmoid.

For each combination of Atlas and Functional Connectivity Measures, Convolutional Neural Networks were tested using the following activation functions: Rectified Linear Unit (ReLU), Hyperbolic Tangent (tanh), and Leaky Rectified Linear Unit (Leaky ReLU). The architecture of the simple CNN model is as follows: one convolutional layer with 16 filters and a kernel size of 2 x 2, followed by a dropout layer to mitigate overfitting with a dropout rate 20%. A pooling layer is used to summarise the features present in each set of filters

which are then flattened into a vector representation and fed into the output layer directly. The output layer consists of two units to represent each of the two classes. Categorical cross-entropy was used as the loss function, the learning rate was set to 0.005, and the Adam optimizer was used. Each model was trained for 75 epochs with a batch size of 100. A plot of the proposed CNN model is shown in Figure 10.

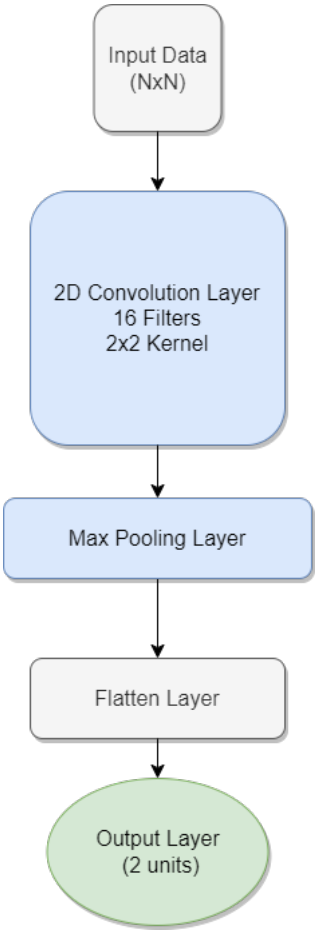

Figure 10: A plot of the CNN model architecture. N represents the number of ROIs present in the atlas used as input.

CHAPTER IV.

RESULTS

All models were evaluated using the average accuracy, area under the curve-receiver operating characteristics (AUC), precision, and recall through a rigorous 10-fold cross-validation approach, repeated five times with data shuffling for each iteration. This comprehensive assessment explored the predictive capability of the AAL, cc200, and cc400 ROI atlases concerning various functional connectivity measures, including Pearson correlation, tangent, covariance, partial correlation, and precision. All confidence intervals are calculated at a confidence level of 95%. The tables and figures shown below represent the tests with the highest accuracy for each combination of atlas and functional connectivity measure.

Convolutional Neural Network Model Results

Table 2 and Figure 11 show the best accuracies of the CNN models for each activation function. Table 10, located in Appendix A, contains the results for all tests. The accuracy is defined as the percentage of correct classifications. The highest accuracy for the AAL atlas uses the tangent functional connectivity measure and achieves an accuracy of 63.13%. The highest accuracy for the cc200 atlas uses the Pearson correlation functional connectivity measure and achieves an accuracy of 66.27%. The highest accuracy for the cc400 atlas used the Pearson correlation functional connectivity measure and achieved an accuracy of 68.11%. Figure 15, located in Appendix B, gives a graphical comparison for the accuracies of all tests performed on the AAL, cc200, and cc400 atlases.

Table 2: The Accuracy for the best tests for each connectivity measure and atlas combination, using the proposed CNN model and confidence intervals with a confidence of 95%

Functional Connectivity Measure	AAL	cc200	400
Correlation	0.6219 ± 0.0148	$\mathbf{0.6627 \pm 0.0155}$	$\mathbf{0.6811 \pm 0.0149}$
Tangent	$\mathbf{0.6313 \pm 0.0144}$	0.6451 ± 0.0131	0.6370 ± 0.0146
Covariance	0.5791 ± 0.0130	0.5925 ± 0.0160	0.6430 ± 0.0150
Partial Correlation	0.6050 ± 0.0144	0.5775 ± 0.0119	0.5929 ± 0.0129
Precision	0.5373 ± 0.0135	0.5373 ± 0.0135	0.5373 ± 0.0135

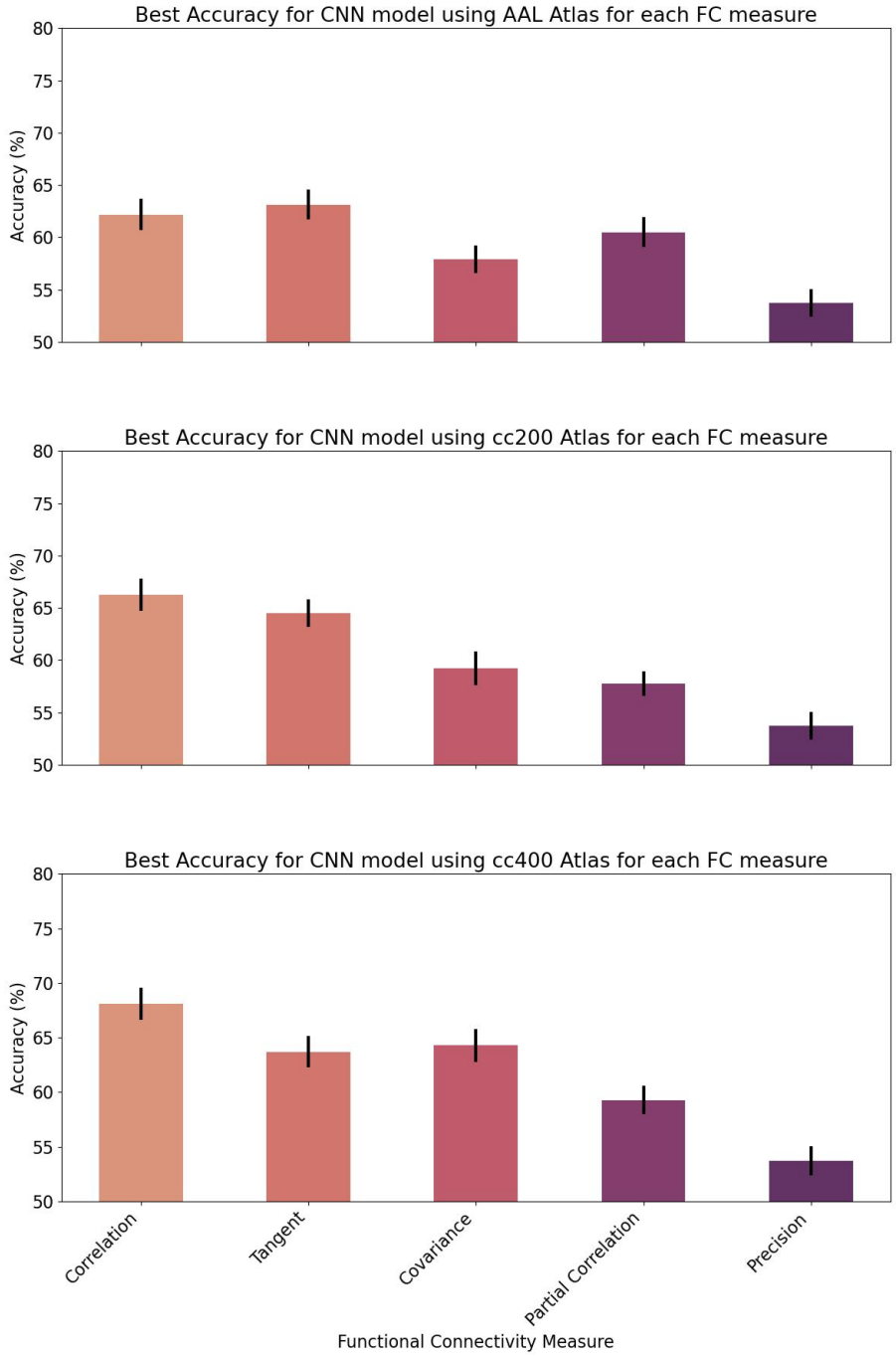

Figure 11: The best Accuracy for the CNN model using each connectivity measure for the AAL, cc200, and cc400 atlases

Table 3 and Figure 12 shows the Area Under the Curve score (AUC) for the most accurate CNN models using the AAL, cc200, and cc400 atlases. Table 11, located in Appendix A, contains the AUC scores for all tests. The AUC score assesses the model's capability to accurately differentiate between the two classes. It accomplishes this by plotting the True Positive Rate against the False Positive Rate across various confidence thresholds used to classify an item as positive. The tests with the highest AUC scores are in line with the most accurate tests for each atlas. The AUC score for the most accurate model using the AAL atlas achieves a score of 0.6829. The highest AUC for the most accurate model using the cc200 atlas achieved a score of 0.7193. The highest AUC for the most accurate model using the cc400 atlas achieved a score of 0.7345. Figure 16, located in Appendix C, gives a graphical comparison for the AUC scores of all tests performed on the AAL, cc200, and cc400 atlases respectively.

Table 3: The AUC scores for the tests with the best accuracy for each combination of brain atlas and connectivity measure using the proposed CNN model. Confidence intervals are calculated at 95%

FC Measure	AAL	cc200	cc400
Correlation	0.6593 ± 0.0160	$\mathbf{0.7193 \pm 0.0162}$	$\mathbf{0.7345 \pm 0.0150}$
Tangent	$\mathbf{0.6829 \pm 0.0151}$	0.7040 ± 0.0131	0.6994 ± 0.0147
Covariance	0.5809 ± 0.0129	0.5932 ± 0.0162	0.6578 ± 0.0152
Partial Correlation	0.6462 ± 0.0159	0.6065 ± 0.0121	0.6269 ± 0.0140
Precision	0.5373 ± 0.0135	0.5373 ± 0.0135	0.5373 ± 0.0135

Table 4 shows the recall scores for the AAL, cc200, and cc400 atlases. Table 12, located in Appendix A, contains the recall scores for all tests. The recall score, also known as sensitivity, gives the percentage of the total positive cases that the model correctly identifies. The most accurate CNN model using the AAL atlas achieves a recall of 0.6979. The most accurate model using the cc200 atlas achieves a recall of 0.7162. The most accurate model using the cc400 atlas achieves a recall of 0.7341. Recall is a good metric for models that achieve high accuracies; however, it can also be helpful for interpreting models with overall

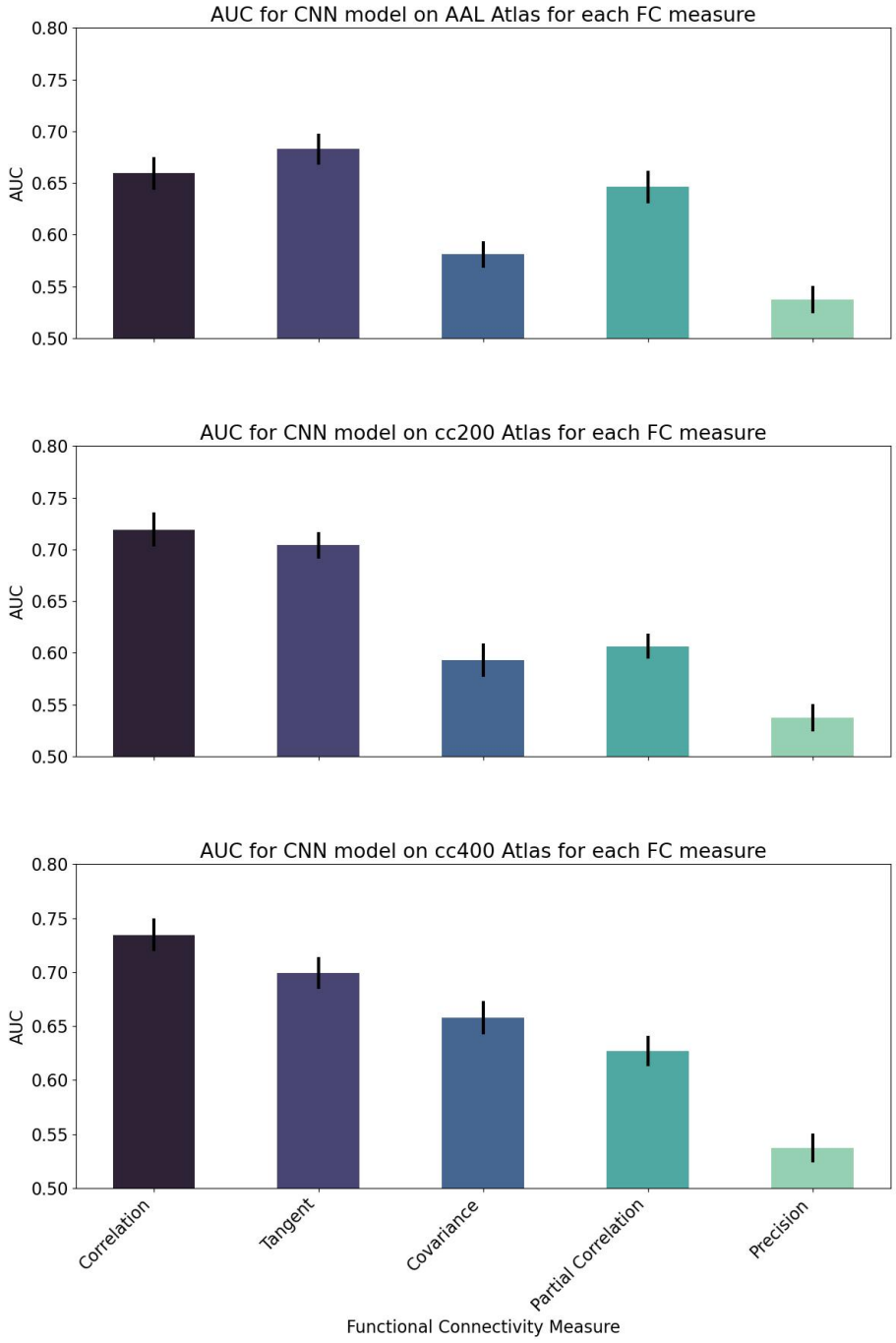

Figure 12: The AUC scores for the most accurate CNN models using each connectivity measure for the AAL, cc200, and cc400 atlases respectively

poor performance. For instance, the precision connectivity measure achieves a recall of 100% across all atlases, but only achieved an accuracy of 53.73%. In this case, the model likely labeled all examples as positive, thus giving it a 100% precision score in spite of having an accuracy that is indicative of a random guess. Figure 17, located in Appendix D gives a graphical comparison for the recall scores of the AAL, cc200, and cc400 tests respectively.

Table 4: The Recall scores for the tests with the best accuracy for each combination of brain atlas and connectivity measures using the proposed CNN model. Confidence intervals are calculated at 95%

FC Measure	AAL	cc200	cc400
Correlation	0.7016 ± 0.0228	$\mathbf{0.7162 \pm 0.0255}$	$\mathbf{0.7341 \pm 0.0185}$
Tangent	$\mathbf{0.6979 \pm 0.0220}$	0.7254 ± 0.0204	0.7518 ± 0.0212
Covariance	0.6250 ± 0.0384	0.5962 ± 0.0344	0.7494 ± 0.0242
Partial Correlation	0.7211 ± 0.0216	0.6929 ± 0.0334	0.7570 ± 0.0366
Precision	1.0000 ± 0.0	1.0000 ± 0.0	1.0000 ± 0.0

Table 5: The Precision scores for the tests with the best accuracy for each combination of brain atlas and connectivity measures using the proposed CNN model. Confidence intervals are calculated at 95%

FC Measure	AAL	cc200	cc400
Correlation	0.6354 ± 0.0181	$\mathbf{0.6801 \pm 0.0196}$	$\mathbf{0.6927 \pm 0.0188}$
Tangent	$\mathbf{0.6470 \pm 0.0184}$	0.6547 ± 0.0174	0.6414 ± 0.0193
Covariance	0.6068 ± 0.0185	0.6293 ± 0.0194	0.6473 ± 0.0200
Partial Correlation	0.6157 ± 0.0194	0.5971 ± 0.0177	0.6027 ± 0.0183
Precision	0.5373 ± 0.0135	0.5373 ± 0.0135	0.5373 ± 0.0135

Table 5 shows the Precision for the AAL, cc200, and cc400 atlases. Table 13, located in Appendix A, contains the results for all tests. Precision measures the percent of positive predictions made that were correctly classified as positive. The most accurate CNN model using the AAL atlas achieves a precision of 0.6470. The most accurate model using the cc200 atlas achieves a precision of 0.6801. The most accurate model using the cc400 atlas achieves a precision of 0.6927. Figure 18, located in Appendix E, graphically represents the

precision scores for the AAL, cc200, and cc400 atlases respectively.

Support Vector Machine Results

Table 6 and Figure 13 show the best average accuracies achieved by the support vector machines for the AAL, cc200, and cc400 atlases across all connectivity measures. Table 14, located in Appendix F, contains the results for all tests. The best accuracy for the SVM model with the AAL atlas was 65.9% using the Pearson correlation functional connectivity measure. The best accuracy for the SVM model on the cc200 atlas was 69.41% using the Pearson correlation functional connectivity measure. The best accuracy for the SVM model using the cc400 atlas was 69.62% using the Pearson correlation functional connectivity measure. Figure 19, located in Appendix G, compares the average accuracy for all tests on the AAL, cc200, and cc400 atlases respectively.

Table 6: The best accuracies for SVM tests using each functional connectivity measure for each atlas. Confidence intervals are calculated to be 95%

FC Measure	AAL	cc200	cc400
Correlation	**0.659 ± 0.0149**	**0.6941 ± 0.0144**	**0.6962 ± 0.0127**
Tangent	0.6583 ± 0.0152	0.6675 ± 0.0151	0.6709 ± 0.0148
Covariance	0.6583 ± 0.0152	0.6393 ± 0.0148	0.6447 ± 0.0144
Partial Correlation	0.6080 ± 0.0144	0.6259 ± 0.0151	0.6229 ± 0.0160
Precision	0.5991 ± 0.0147	0.6101 ± 0.0151	0.6172 ± 0.0163

Table 7 and Figure 14 show the average AUC scores achieved by the most accurate support vector machine models for the AAL, cc200, and cc400 atlases across all connectivity measures. Table 15, located in Appendix F, contains the results for all tests. The best AUC score for the most accurate SVM test using the AAL atlas is 0.653. The best AUC score for the most accurate SVM test using the cc200 atlas was 0.691. The best AUC score for the most accurate SVM test using the cc400 atlas was 0.692. Figure 20, located in Appendix H, graphically compares the average AUC score for all tests for the AAL, cc200, and cc400 atlases respectively.

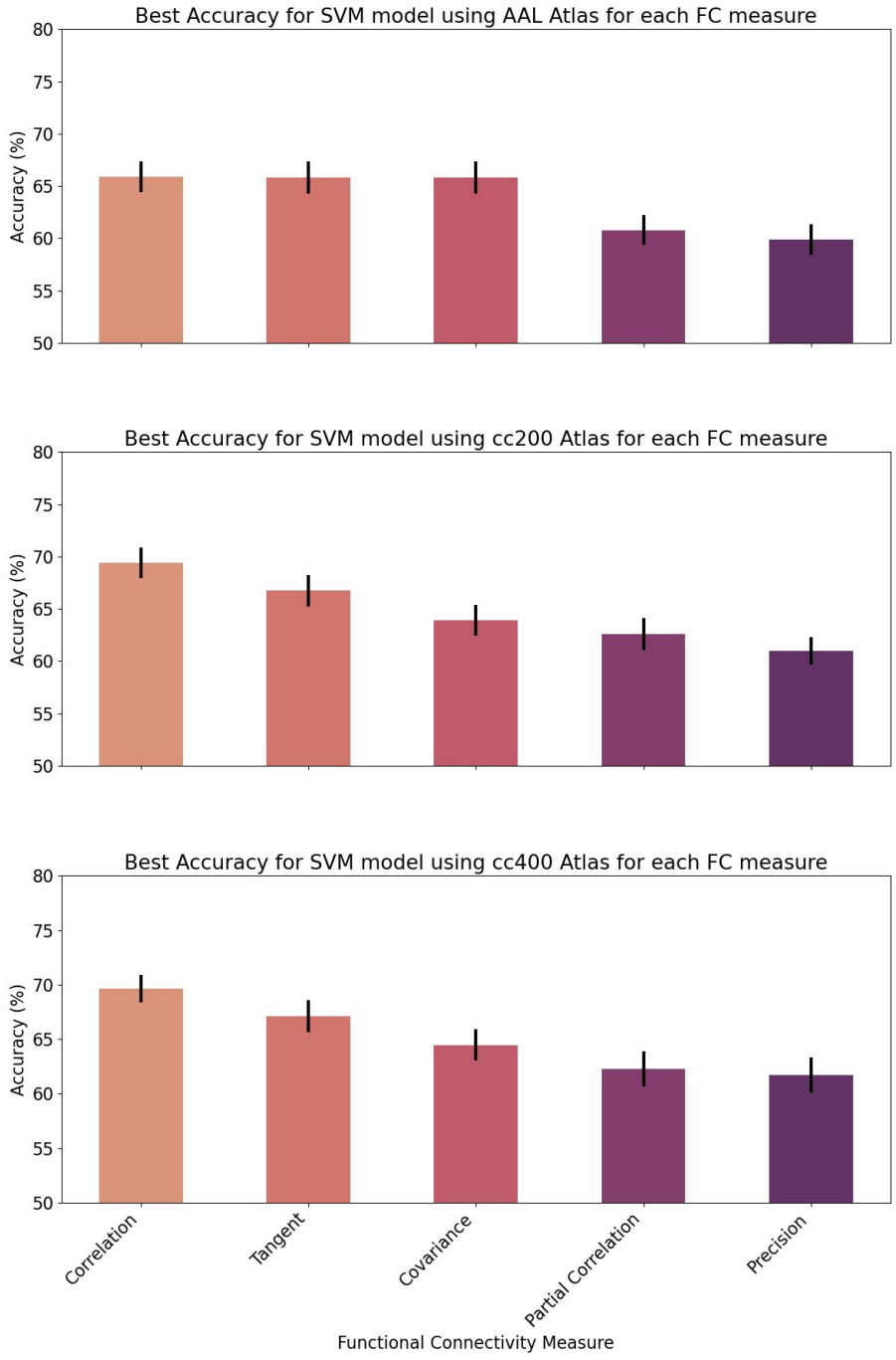

Figure 13: The best accuracy for the SVM model using each connectivity measure for the AAL, cc200, and cc400 atlases

Table 7: The AUC scores for SVM tests with the highest average accuracy using each functional connectivity measure for each atlas. Confidence intervals are calculated to be 95%

FC Measure	AAL	cc200	cc400
Correlation	**0.653 ± 0.015**	**0.691 ± 0.014**	**0.692 ± 0.013**
Tangent	0.655 ± 0.015	0.662 ± 0.015	0.664 ± 0.015
Covariance	0.655 ± 0.015	0.638 ± 0.015	0.644 ± 0.015
Partial Correlation	0.602 ± 0.015	0.617 ± 0.015	0.612 ± 0.016
Precision	0.597 ± 0.015	0.604 ± 0.013	0.607 ± 0.017

Table 8 shows the best average recall scores achieved by the most accurate support vector machine models for the AAL, cc200, and cc400 atlases for each connectivity measure. Table 16, located in Appendix F, contains the results for all tests. The recall score for the most accurate SVM model using the AAL atlas was 0.575. The recall score for the most accurate SVM model using the cc200 atlas was 0.648. The Recall score for the most accurate SVM model using the cc400 atlas was 0.643. Figure 21, located in Appendix I, compares the average recall score for all tests for the AAL, cc200, and cc400 atlases respectively.

Table 8: The Recall scores for SVM tests with the highest average accuracy using each functional connectivity measure for each atlas. Confidence intervals are calculated to be 95%

FC Measure	AAL	cc200	cc400
Correlation	**0.575 ± 0.018**	**0.648 ± 0.020**	**0.643 ± 0.022**
Tangent	0.604 ± 0.022	0.593 ± 0.023	0.577 ± 0.025
Covariance	0.604 ± 0.022	0.620 ± 0.023	0.633 ± 0.022
Partial Correlation	0.520 ± 0.023	0.492 ± 0.023	0.464 ± 0.025
Precision	0.563 ± 0.022	0.522 ± 0.019	0.473 ± 0.028

Table 9 shows the average precision scores achieved by the most accurate support vector machine models for the AAL, cc200, and cc400 atlases for each connectivity measure. Table 17, located in Appendix F, contains the results for all tests. The precision score for the most accurate SVM model using the AAL atlas was 0.652. The precision score for the

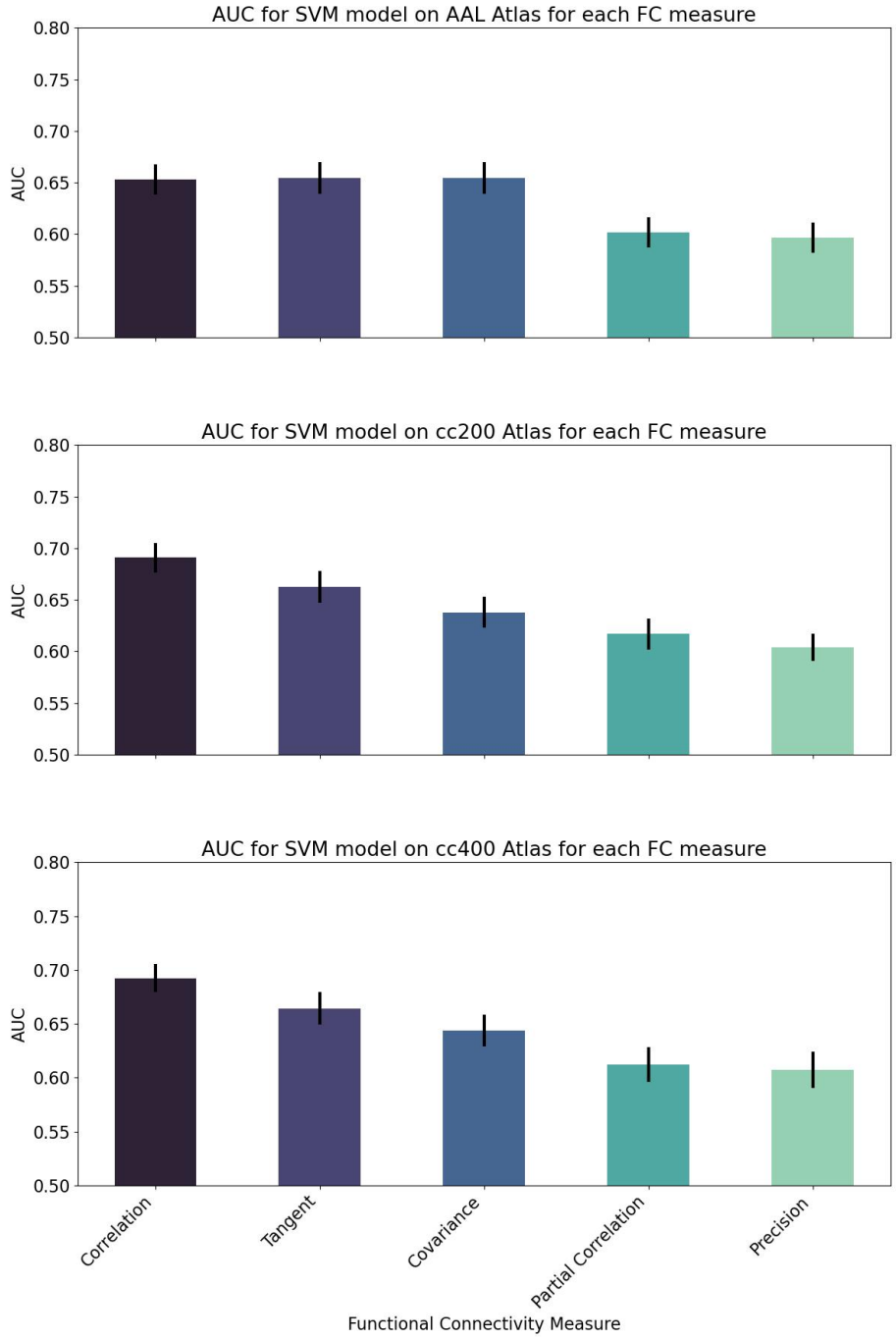

Figure 14: The AUC scores for the most Accurate models using each connectivity measure for the AAL, cc200, and cc400 atlases respectively

most accurate SVM model using the cc200 atlas was 0.68. The precision score for the most accurate cc400 atlas was 0.683. Figure 22, located in Appendix J, compares the average recall score for all tests using the AAL, cc200, and cc400 atlases respectively.

Table 9: The Precision scores for SVM tests with the highest average accuracy using each functional connectivity measure for each atlas. Confidence intervals are calculated to be 95%

FC Measure	AAL	cc200	cc400
Correlation	**0.652 ± 0.020**	**0.680 ± 0.018**	**0.683 ± 0.014**
Tangent	0.639 ± 0.018	0.658 ± 0.019	0.667 ± 0.018
Covariance	0.639 ± 0.018	0.609 ± 0.016	0.613 ± 0.015
Partial Correlation	0.586 ± 0.018	0.625 ± 0.022	0.626 ± 0.024
Precision	0.568 ± 0.016	0.590 ± 0.016	0.610 ± 0.021

CHAPTER V.

DISCUSSION

In this section, the proposed CNN model will be compared to previous CNN models used in the literature. The proposed model will also be compared to SVMs, as they are commonly used for classification tasks using functional connectivity measures. Then each atlas and functional connectivity measure will be compared to one another to determine which are most suitable for ASD detection.

Proposed Convolutional Neural Network Model

As shown in Table 2, the best overall average accuracy was 68.11% $\pm$ 1.49%. Therefore, the true mean is between 66.62%-69.6% with a confidence of 95%. The measured accuracy does not exceed the state of the art of 73.1% as reported by Khosla et. al [13]. The AUC reported by Khosla et. al is 75.8% compared to our proposed model's AUC score of 73.45% $\pm$ 1.5%. Khosla et. al did not report the confidence intervals for their proposed model, consequently, the models cannot be compared with statistical significance. Further testing will be needed to determine if the difference in the accuracies and AUC scores of the two models is significant.

While the highest average accuracy for this proposed model is 68.11% for the cc400 atlas with the Pearson correlation functional connectivity measure, the cc200 atlas provides comparable accuracies. The highest accuracy for the cc200 atlas is 67.1% $\pm$ 1.411%. Because the difference in performance of these two models is statistically insignificant and the cc200 atlas has fewer features, using the cc200 atlas for this model offers some substantial benefits in space and time complexity without sacrificing performance. The proposed model using the cc400 atlas has 1,216,882 parameters, while the proposed model using the cc200 atlas has 313,714 parameters resulting in approximately a 74% decrease in the size of the model. Both of these models have fewer parameters than the state-of-the-art CNN models for detecting ASD. The model reported by Sherkatghanad et. al has 4,398,802

parameters with an accuracy of 70.22%. The model proposed by Xing et. al used 1,268,160 parameters and has a reported accuracy of 66.88%, making the CNN model proposed in this study less complex than both models while having similar accuracies. Khosla et. al did not report the number of parameters used in their proposed models [14, 17, 13].

The best accuracy for the SVM model for detecting ASD is 69.6% $\pm$ 1.27% and uses the Pearson correlation functional connectivity measure as shown in table 6. The observed results show overlapping confidence intervals between the SVM tests and the proposed CNN model; therefore, the difference in the accuracies is concluded to be statistically insignificant.

Atlas Comparison

Each atlas will be compared using the results found from the SVM model as well as the proposed CNN model.

The cc200 and cc400 atlases had similar performances when using the SVM model, with the best accuracy for the cc200 atlas being 69.41% $\pm$ 1.4% and the best accuracy for the cc400 atlas being 69.6% $\pm$ 1.1% as shown in Table 6. Both atlases also performed similarly for AUC, precision, and recall with their highest performing model for each metric being statistically similar as shown in Tables 7, 8, and 9. Both of these atlases provide a similar level of predictive value despite the cc400 atlas having twice the ROIs. This means that the cc200 atlas would provide a significant advantage in terms of space complexity which could translate to a faster fitting and prediction time given similar hardware. As the hardware for this study was not controlled, fit times were not tracked for comparison.

The AAL atlas performed the worst of the three atlases when using the SVM model. The highest accuracy achieved by the AAL atlas was 65.8% $\pm$ 1.5%. The AAL atlas does not show the same predictive capabilities as the cc200 or cc400 atlases for use in SVMs as shown in tables 6, 7, 8, and 9.

The same trends were shown with the proposed CNN model. The difference between

the best accuracies found for the CNN model using the cc200 and cc400 are not statistically significant; therefore, we cannot determine that one is more useful for detecting ASD with this model. The best-performing CNN model using the AAL atlas has an accuracy of 63.12% $\pm$ 1.44% using the Tangent connectivity measure. This shows that the AAL atlas has less predictive capacity than the cc200 and cc400 atlases when using SVMs and the proposed CNN model.

Functional Connectivity Measure Comparison

Each connectivity was tested to determine its predictive capacity for each atlas using both SVMs and the proposed CNN model.

The most effective functional connectivity measure for the cc200 and cc400 atlases is the Pearson correlation measure as shown in table 6. This substantiates the overall prevalence of the use of the Pearson correlation measure across the literature [11, 13, 14, 17, 16]. The best accuracy for the Pearson correlation measure using the SVM on the cc200 atlas was 69.41% $\pm$ 1.44% and on the cc400 atlas was 69.62% $\pm$ 1.27%. The Pearson Correlation has the best accuracy for the AAL atlas at 65.90% $\pm$ 1.49%, as shown in table 6. The difference between Pearson Correlation and the next best accuracy – which is a tie between the covariance and tangent functional connectivity measures – is statistically insignificant.

The Tangent functional connectivity measure also showed promise as a predictive measure for SVMs. When using SVMs on the cc400 atlas, the tangent functional connectivity measure showed to be statistically similar to the Pearson measure with an accuracy of 67.09 $\pm$ 1.48%. For tests on the cc200 atlas, the tangent measure has an accuracy of 66.75% $\pm$ 1.51% which is statistically similar to the performance of the Pearson correlation measure for the SVM using the cc200 atlas. Therefore, for the cc200 atlas, the tangent functional connectivity measure has a comparable amount of predictive capability as the Pearson correlation measure. This is also true for the AAL atlas where the Tangent measure achieves an accuracy of 65.83% $\pm$ 1.52% placing it on par with the second best-performing

connectivity measures for the AAL atlas.

Conversely, the covariance functional connectivity measure achieved a mixed bag of results. For the AAL atlas, the second best score using the SVMs uses the Covariance functional connectivity measure using the RBF kernel with an accuracy of 65.83% $\pm$ 1.52%. This is the only test in which the covariance connectivity measure is able to perform comparably to the correlation or tangent measures. For the cc200 and cc400 atlases the covariance functional connectivity measure does not perform as well as the correlation or the tangent functional connectivity measures with accuracies of 63.93% $\pm$ 1.48% and 64.47% $\pm$ 1.44% respectively.

The partial correlation and precision functional connectivity measures both performed the worst for all atlases. For the cc200 and cc400 atlases, the difference between partial correlation and covariance was not statistically significant, but the tangent and correlation connectivity measures both perform significantly better than partial correlation. The precision connectivity measure performs the weakest for all atlases. The precision functional connectivity measure achieves high recall scores, but these do not correspond to high accuracies. It is observed that the models created on precision scores tended to over-bias towards classifying a subject as ASD-positive.

For the proposed CNN model, Pearson correlation also achieves best accuracy for the cc200 and cc400 atlases, whereas the tangent connectivity measure has the highest accuracy for the AAL atlas. For the cc200 and the AAL atlases, the difference in the average accuracy of the Pearson correlation and tangent functional connectivity measure are statistically insignificant. The covariance connectivity measure does not perform well for the CNN model using the cc200 atlas; however, when used in conjunction with the AAL and the cc400 atlases for the proposed model, it is observed to be an effective connectivity measure for detecting ASD. Partial correlation and precision, much like when used for SVMs, performed the worst for all atlases.

CHAPTER VI.

CONCLUSION

In this study, a simple CNN architecture was developed to classify fMRIs as ASD-positive or typically developing. The proposed model is able to achieve a similar accuracy as SVMs and several other proposed CNN-based models while having fewer parameters; however, the proposed model was not able to achieve the same accuracies as the state-of-the-art CNN based model [13]. In addition, both SVMs and the proposed CNN model were used to test the predictive capacity of the AAL, cc200, and cc400 atlases in combination with the Pearson correlation, tangent, partial correlation, covariance, and precision functional connectivity measures. The cc200 and the cc400 atlases were able to achieve greater accuracies than the AAL atlas. While the Pearson correlation is the most widely used connectivity measure, there were some cases in which using the tangent or covariance functional connectivity measures produced similar if not better results. We conclude that models should be tested using the tangent and covariance connectivity measures as well as Pearson correlation, as it could increase the performance of some models. While the current state of ASD diagnosis using fMRIs is not an effective measure on its own, continued advancements in this area of research could pave the way for the development of new ASD testing methodologies, utilizing fMRIs as a tool to detect potential biomarkers. Continued development will allow doctors to make early ASD diagnoses with higher levels of confidence.

CHAPTER VII.

FUTURE WORK

There are several ways in which this work could be used in future studies of ASD diagnosis. Support Vector Machines can be harnessed with multiple kernel functions to assess the predictive capability of functional connectivity measurements derived from fMRI data. This may result in an SVM being able to derive more information from an fMRI image. Additionally, we suggest utilizing Convolutional Neural Networks' ability to harness multiple channels of data to deduce more information using multiple connectivity measures as inspired by models proposed by Khosla et. al [13]. This could be a way to utilize multiple methods of extracting useful information from an fMRI and give more information to train the CNN model which may lead to better outcomes. We also suggest utilizing a joint CNN-SVM model similar to the one proposed by T. Eslami and F. Saeed [11]. Additionally, there is further work to be done in comparing connectivity measures for different brain atlases that were not tested in this study.

BIBLIOGRAPHY

[1] American Psychiatric Association, "Diagnostic and Statistical Manual of Mental Disorders." DSM Library. Accessed: Nov. 16, 2023.

[2] Center for Disease Control (CDC), "Autism spectrum disorder (asd) — cdc," 2023.

[3] Autism Speaks, "Autism statistics and facts," 2023. Accessed: Jun. 01, 2023.

[4] Center for Disease Control (CDC), "Autism Data Visualization Tool — CDC," 2023.

[5] S. L. Hyman et al., "Identification, evaluation, and management of children with autism spectrum disorder," *Pediatrics*, vol. 145, p. e20193447, Jan 2020.

[6] P. McCarty and R. Frye, "Early detection and diagnosis of autism spectrum disorder: Why is it so difficult?," *Seminars in Pediatric Neurology vol. 25, p. 100831*, 2020.

[7] G. H. Glover, "Overview of functional magnetic resonance imaging," *Neurosurgery Clinic of North America*, vol. vol. 22.

[8] D. Sadeghi et al., "An overview of artificial intelligence techniques for diagnosis of schizophrenia based on magnetic resonance imaging modalities: Methods, challenges, and future works," *Computers in Biology and Medicine, vol. 146, p. 105554*, 2022.

[9] Y. Bae, K. Kumarasamy, I. M. Ali, P. Korfiatis, Z. Akkus, and B. J. Erickson, "Differences Between Schizophrenic and Normal Subjects Using Network Properties from fMRI," *J Digit Imaging, vol. 31, no. 2, pp. 252–261*, 2018.

[10] A. Riaz et al., "Deep fMRI: AN end-to-end deep network for classification of fMRI data," *International Symposium on Biomedical Imaging (ISBI 2018)*, 2018.

[11] T. Eslami and F. Saeed, "Auto-asd-network: A technique based on deep learning and support vector machines for diagnosing autism spectrum disorder using fmri data," *ACM*.

[12] R. Ju, C. Hu, Pan Zhou, Q. Li, "Early diagnosis of alzheimer's disease based on resting-state brain networks and deep learning," *IEEE/ACM Transactions on Computational Biology and Bioinformatics*, vol. 16, pp. 244–257, Jan 2019.

[13] M. Khosla, K. Jamison and A. Kuceyeski and M. R. Sabuncu, "3D Convolutional Neural Networks for Classification of Functional Connectomes," in *Deep Learning in Medical Image Analysis and Multimodal Learning for Clinical Decision Support* (D. Stoyanov, Z. Taylor, G. Carneiro, T. Syeda-Mahmood, A. Martel and L. Maier-Hein and J. M. R. S. Tavares and A. Bradley and J. P. Papa and V. Belagiannis and J. C. Nascimento and Z. Lu and S. Conjeti and M. Moradi and H. Greenspan and A. Madabhushi, ed.), Lecture Notes in Computer Science, pp. 137–145, Springer International Publishing, 2018.

[14] Z. e. a. Sherkatghanad, "Automated detection of autism spectrum disorder using a convolutional neural network," *Frontiers in Neuroscience*, vol. 13, 2020. Accessed: Jun. 30, 2023.

[15] H. Ahmadi, E. Fatemizadeh, A. Motie-Nasrabadi, "A Comparative Study of Correlation Methods in Functional Connectivity Analysis Using fMRI Data of Alzheimer's Patients," *J Biomed Phys Eng*, vol. 13, pp. 125–134, Apr 2023.

[16] X. Yang and N. Zhang, "A deep neural network study of the abide repository on autism spectrum classification," *International Journal of Advanced Computer Science and Applications*, 2020.

[17] X. Xing, J. Ji, and Y. Yao, "Convolutional Neural Network with Element-wise Filters to Extract Hierarchical Topological Features for Brain Networks," in *2018 IEEE International Conference on Bioinformatics and Biomedicine (BIBM)*, pp. 780–783, Dec 2018.

[18] Cameron Craddock, , "The neuro bureau preprocessing initiative: open sharing of preprocessed neuroimaging data and derivatives," *Frontiers in Neuroinformatics*.

[19] A. S. Heinsfeld, A. R. Franco, R. C. Craddock, A. Buchweitz, and F. Meneguzzi, "Identification of autism spectrum disorder using deep learning and the ABIDE dataset," *NeuroImage: Clinical, vol. 17, pp. 16–23*, 2018.

[20] A. Abraham, F. Pedregosa, M. Eickenberg, P. Gervais, A. Mueller, J. Kossaifi, B. and Thirion, and G. Varoquaux, "Machine Learning for Neuroimaging with Scikit-Learn," *Frontiers in Neuroinformatics*, vol. 8, 2014. Accessed: Oct. 24, 2023.

[21] Craddock, C. et. al, "Towards automated analysis of connectomes: The configurable pipeline for the analysis of connectomes (c-pac)," *Frontiers in Neuroinformatics*, vol. 7, 2013.

[22] T. M. Schouten et al., "Combining anatomical, diffusion, and resting state functional magnetic resonance imaging for individual classification of mild and moderate Alzheimer's disease," *NeuroImage: Clinical, vol. 11, pp. 46–51*, 2016.

[23] A. Khazaee, A. Ebrahimzadeh, and A. Babajani-Feremi, "Application of advanced machine learning methods on resting-state fmri network for identification of mild cognitive impairment and alzheimer's disease," *Brain Imaging and Behavior, vol. 10, no. 3, pp. 799–817*, 2016.

[24] M. J. Rosa et al., "Sparse network-based models for patient classification using fMRI," *NeuroImage, vol. 105, pp. 493–506*, 2015.

[25] R. C. Craddock, G. A. James, P. E. Holtzheimer III, X. P. Hu, and H. S. Mayberg, "A whole brain fMRI atlas generated via spatially constrained spectral clustering," *Human Brain Mapping, vol. 33, no. 8, pp. 1914–1928*, 2012.

[26] X. Yang, N. Zhang, and P. Schrader, "A study of brain networks for autism spectrum disorder classification using resting-state functional connectivity," *Machine Learning with Applications, vol. 8, p. 100290*, 2022.

[27] W. Yin, L. Li, and F. Wu, "Deep learning for brain disorder diagnosis based on fmri images," *Neurocomputing vol. 469 pp. 332-345*, 2022.

[28] U. Pervaiz, D. Vidaurre, M. W. Woolrich, and S. M. Smith, "Optimising network modelling methods for fmri," *NeuroImage*, vol. 211, p. 116604, May 2020.

[29] O. Ledoit and M. Wolf, "A Well-Conditioned Estimator for Large-Dimensional Covariance Matrices," *Journal of Multivariate Analysis*, vol. 88, pp. 365–411, Feb 2004.

[30] A. Krishnamoorthy and D. Menon, "Matrix inversion using cholesky decomposition," in *Signal Processing - Algorithms, Architectures, Arrangements, and Applications Conference Proceedings*, pp. 70–72, 2013.

[31] G. Varoquaux, F. Baronnet, A. Kleinschmidt, P. Fillard, and B. Thirion, "Detection of Brain Functional-Connectivity Difference in Post-Stroke Patients Using Group-Level Covariance Modeling," in *Lecture Notes in Computer Science*, vol. 6361, pp. 200–208, 2010.

[32] J. Cervantes, F. Garcia-Lamont, L. Rodríguez-Mazahua, and A. Lopez, "A comprehensive survey on support vector machine classification: Applications, challenges and trends," *Neurocomputing vol. 408, pp. 189-215*, 2020.

[33] A. Patle and D. S. Chouhan, "SVM Kernel Functions for Classification," *2013 International Conference on Advances in Technology and Engineering (ICATE)*, pp. 1–9, Jan 2013.

[34] S. Peltier, J. Lisinski, D. Noll, and S. LlaConte, "Support vector machine classification of complex fmri data," *IEEE*, 2009.

[35] S. H. Hojjati, A. Ebrahimzadeh, A. Khazaee, and A. Babajani-Feremi, "Predicting conversion from mci to ad using resting-state fmri, graph theoretical approach and svm," *Journal of Neuroscience Methods, vol. 282, pp. 69–80*, 2017.

[36] S. Song, Z. Zhan, Z. Long, J. Zhang, and L. Yao, "Comparative study of svm methods combined with voxel selection for object category classification on fmri data," *PLOS ONE, vol. 6, no. 2, p. e17191*, 2011.

[37] Z. Li, F. Liu, W. Yang, S. Peng, and J. Zhou, "A survey of convolutional neural networks: Analysis, applications, and prospects," *IEEE Transactions on Neural Networks and Learning Systems*, vol. 33, no. 12, pp. 6999–7019, 2022.

[38] M. Niepert, M. Ahmed, and K. Kutzkov, "Learning convolutional neural networks for graphs," in *Proceedings of The 33rd International Conference on Machine Learning*, pp. 2014–2023, PMLR, Jun. 2016. Accessed: Oct. 17, 2023.

APPENDICES

APPENDIX A: COMPLETE CNN TEST TABLES

Table 10: The Accuracy for each test using the proposed CNN model and confidence intervals with a confidence of 95%

FC Measure-Activation	AAL	cc200	cc400
Correlation-Relu	0.5901 ± 0.0145	0.6111 ± 0.0149	0.6659 ± 0.0125
Correlation-Tanh	0.6219 ± 0.0148	0.6627 ± 0.0155	0.6811 ± 0.0149
Correlation-Leaky	0.6067 ± 0.0166	0.6453 ± 0.0144	0.6629 ± 0.0138
Tangent-Relu	0.6148 ± 0.0132	0.6104 ± 0.0144	0.6336 ± 0.0123
Tangent-Tanh	0.6313 ± 0.0144	0.6451 ± 0.0131	0.6370 ± 0.0146
Tangent-Leaky	0.6281 ± 0.0145	0.6322 ± 0.0136	0.6333 ± 0.0140
Covariance-Relu	0.5456 ± 0.0149	0.5451 ± 0.0137	0.6363 ± 0.0143
Covariance-Tanh	0.5699 ± 0.0172	0.5805 ± 0.0172	0.6430 ± 0.0150
Covariance-Leaky	0.5791 ± 0.0130	0.5925 ± 0.0160	0.6423 ± 0.0138
Partial Correlation-Relu	0.5612 ± 0.0157	0.5456 ± 0.0173	0.5913 ± 0.0128
Partial Correlation-Tanh	0.6050 ± 0.0144	0.5775 ± 0.0119	0.5902 ± 0.0134
Partial Correlation-Leaky	0.5998 ± 0.0135	0.5449 ± 0.0150	0.5929 ± 0.0129
Precision-Relu	0.5373 ± 0.0135	0.5373 ± 0.0135	0.5373 ± 0.0135
Precision-Tanh	0.5258 ± 0.0158	0.5098 ± 0.0175	0.5155 ± 0.0160
Precision-Leaky	0.5195 ± 0.0163	0.5260 ± 0.0155	0.5314 ± 0.0147

Table 11: The AUC scores for the CNN model for all atlases with a confidence of 95%

FC Measure-Activation	AAL	cc200	cc400
Correlation-Relu	0.6237 ± 0.0157	0.6569 ± 0.0174	0.7193 ± 0.0148
Correlation-Tanh	0.6593 ± 0.0160	0.7193 ± 0.0162	0.7345 ± 0.0150
Correlation-Leaky	0.6446 ± 0.0169	0.7006 ± 0.0154	0.7202 ± 0.0157
Tangent-Relu	0.6582 ± 0.0166	0.6527 ± 0.0175	0.6898 ± 0.0143
Tangent-Tanh	0.6829 ± 0.0151	0.7040 ± 0.0131	0.6994 ± 0.0147
Tangent-Leaky	0.6797 ± 0.0153	0.6836 ± 0.0138	0.6956 ± 0.0143
Covariance-Relu	0.5510 ± 0.0145	0.5485 ± 0.0141	0.6381 ± 0.0144
Covariance-Tanh	0.5810 ± 0.0199	0.5872 ± 0.0190	0.6578 ± 0.0152
Covariance-Leaky	0.5809 ± 0.0129	0.5932 ± 0.0162	0.6437 ± 0.0139
Partial Correlation-Relu	0.5926 ± 0.0155	0.5626 ± 0.0203	0.6334 ± 0.0151
Partial Correlation-Tanh	0.6462 ± 0.0159	0.6065 ± 0.0121	0.6309 ± 0.0146
Partial Correlation-Leaky	0.6386 ± 0.0156	0.5818 ± 0.0151	0.6269 ± 0.0140
Precision-Relu	0.5373 ± 0.0135	0.5373 ± 0.0135	0.5373 ± 0.0135
Precision-Tanh	0.5485 ± 0.0157	0.5254 ± 0.0189	0.5340 ± 0.0163
Precision-Leaky	0.5197 ± 0.0164	0.5263 ± 0.0155	0.5330 ± 0.0148

Table 12: The Recall scores for the CNN model for all atlases with a confidence of 95%

FC Measure-Activation	AAL	cc200	cc400
Correlation-Relu	0.6284 ± 0.0248	0.6519 ± 0.0242	0.7084 ± 0.0182
Correlation-Tanh	0.7016 ± 0.0228	0.7162 ± 0.0255	0.7341 ± 0.0185
Correlation-Leaky	0.7301 ± 0.0309	0.7179 ± 0.0281	0.7182 ± 0.0200
Tangent-Relu	0.6786 ± 0.0213	0.6713 ± 0.0207	0.7504 ± 0.0216
Tangent-Tanh	0.6979 ± 0.0220	0.7254 ± 0.0204	0.7518 ± 0.0212
Tangent-Leaky	0.6912 ± 0.0224	0.7461 ± 0.0321	0.7604 ± 0.0236
Covariance-Relu	0.5529 ± 0.0372	0.5821 ± 0.0236	0.6592 ± 0.0218
Covariance-Tanh	0.6354 ± 0.0757	0.6284 ± 0.0714	0.7494 ± 0.0242
Covariance-Leaky	0.6250 ± 0.0384	0.5962 ± 0.0344	0.7066 ± 0.0223
PartCorrelation-Relu	0.6177 ± 0.0398	0.7348 ± 0.0580	0.7442 ± 0.0294
PartCorrelation-Tanh	0.7211 ± 0.0216	0.6929 ± 0.0334	0.7683 ± 0.0265
PartCorrelation-Leaky	0.6720 ± 0.0503	0.7730 ± 0.0874	0.7570 ± 0.0366
Precision-Relu	1.0000 ± 0.0	1.0000 ± 0.0	1.0000 ± 0.0
Precision-Tanh	0.7397 ± 0.1075	0.6112 ± 0.1333	0.6898 ± 0.1112
Precision-Leaky	0.7800 ± 0.1189	0.8200 ± 0.1103	0.9400 ± 0.0682

Table 13: The Precision Scores for the CNN model for the AAL, cc200, and cc400 atlases

FC Measure-Activation	AAL	cc200	cc400
Correlation-Relu	0.6204 ± 0.0189	0.6358 ± 0.0191	0.6839 ± 0.0179
Correlation-Tanh	0.6354 ± 0.0181	0.6801 ± 0.0196	0.6927 ± 0.0188
Correlation-Leaky	0.6157 ± 0.0199	0.6624 ± 0.0201	0.6764 ± 0.0179
Tangent-Relu	0.6343 ± 0.0190	0.6314 ± 0.0193	0.6370 ± 0.0175
Tangent-Tanh	0.6470 ± 0.0184	0.6547 ± 0.0174	0.6414 ± 0.0193
Tangent-Leaky	0.6459 ± 0.0186	0.6375 ± 0.0165	0.6367 ± 0.0191
Covariance-Relu	0.5834 ± 0.0192	0.5777 ± 0.0194	0.6665 ± 0.0211
Covariance-Tanh	0.5977 ± 0.0336	0.6185 ± 0.0249	0.6473 ± 0.0200
Covariance-Leaky	0.6068 ± 0.0185	0.6293 ± 0.0194	0.6587 ± 0.0187
Partial Correlation-Relu	0.5938 ± 0.0191	0.5650 ± 0.0189	0.6014 ± 0.0175
Partial Correlation-Tanh	0.6157 ± 0.0194	0.5971 ± 0.0177	0.5961 ± 0.0181
Partial Correlation-Leaky	0.6285 ± 0.0208	0.5464 ± 0.0393	0.6027 ± 0.0183
Precision-Relu	0.5373 ± 0.0135	0.5373 ± 0.0135	0.5373 ± 0.0135
Precision-Tanh	0.5027 ± 0.0457	0.4161 ± 0.0814	0.5123 ± 0.0504
Precision-Leaky	0.4184 ± 0.0650	0.4417 ± 0.0604	0.5044 ± 0.0389

APPENDIX B: GRAPHS FOR CNN TESTS ACCURACY

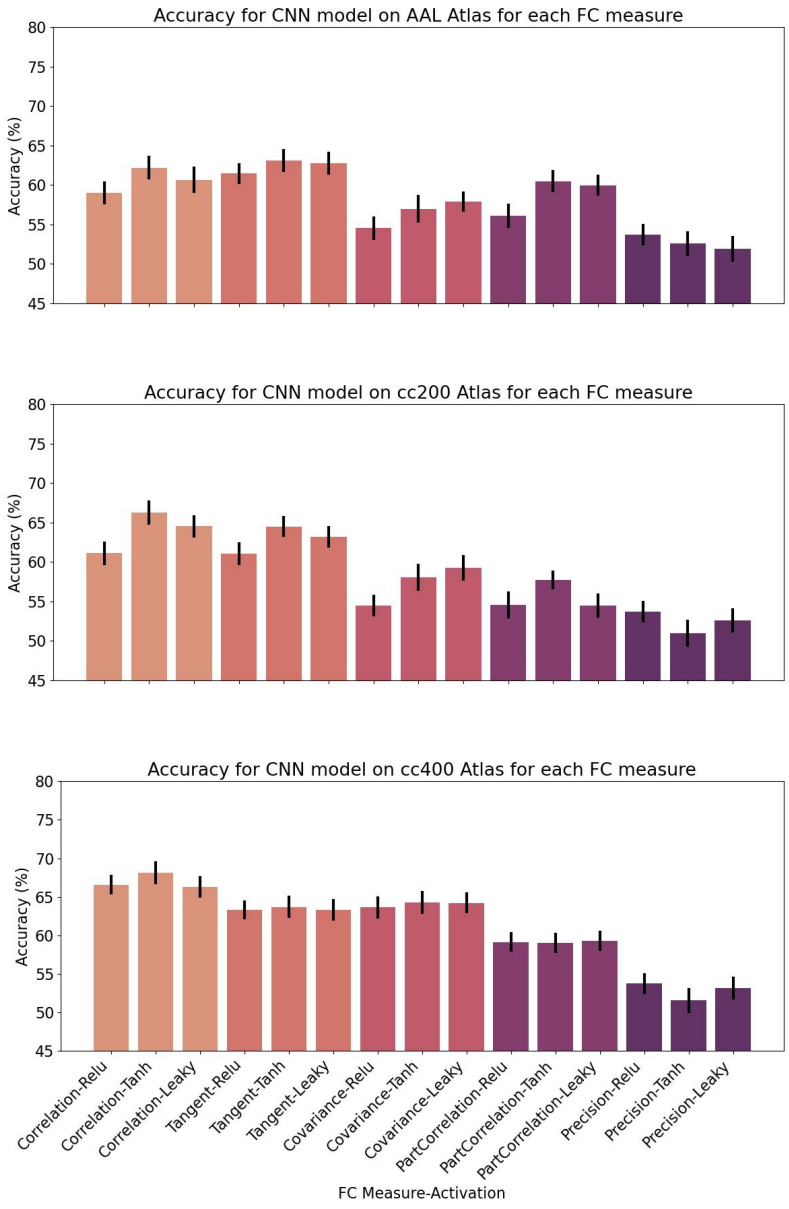

Figure 15: The accuracies of the CNN model using the AAL, cc200, and cc400 atlases

APPENDIX C: GRAPHS FOR CNN TESTS AUC

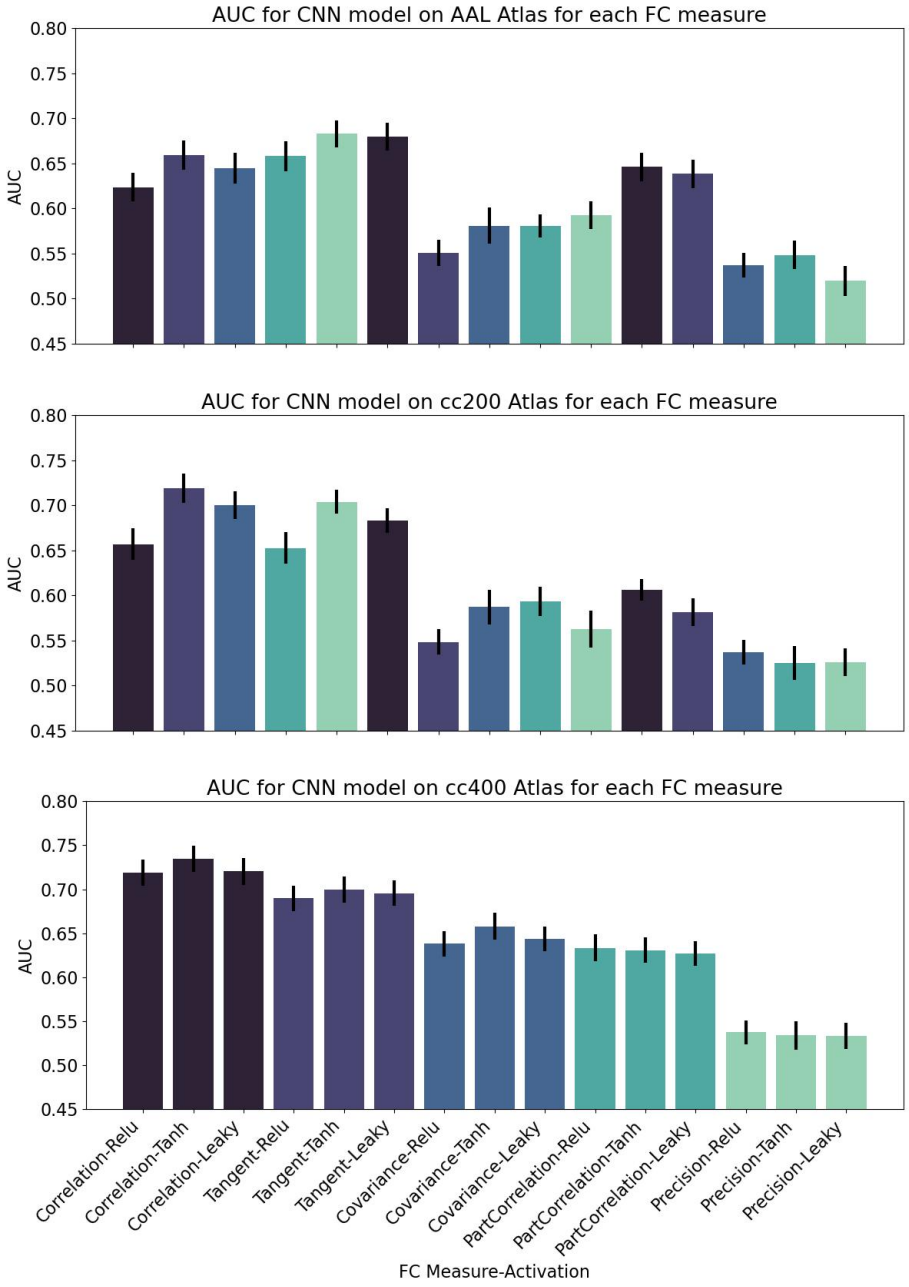

Figure 16: The AUC scores for the CNN model on the AAL, cc200, and cc400 atlases

APPENDIX D: GRAPHS FOR CNN TESTS RECALL

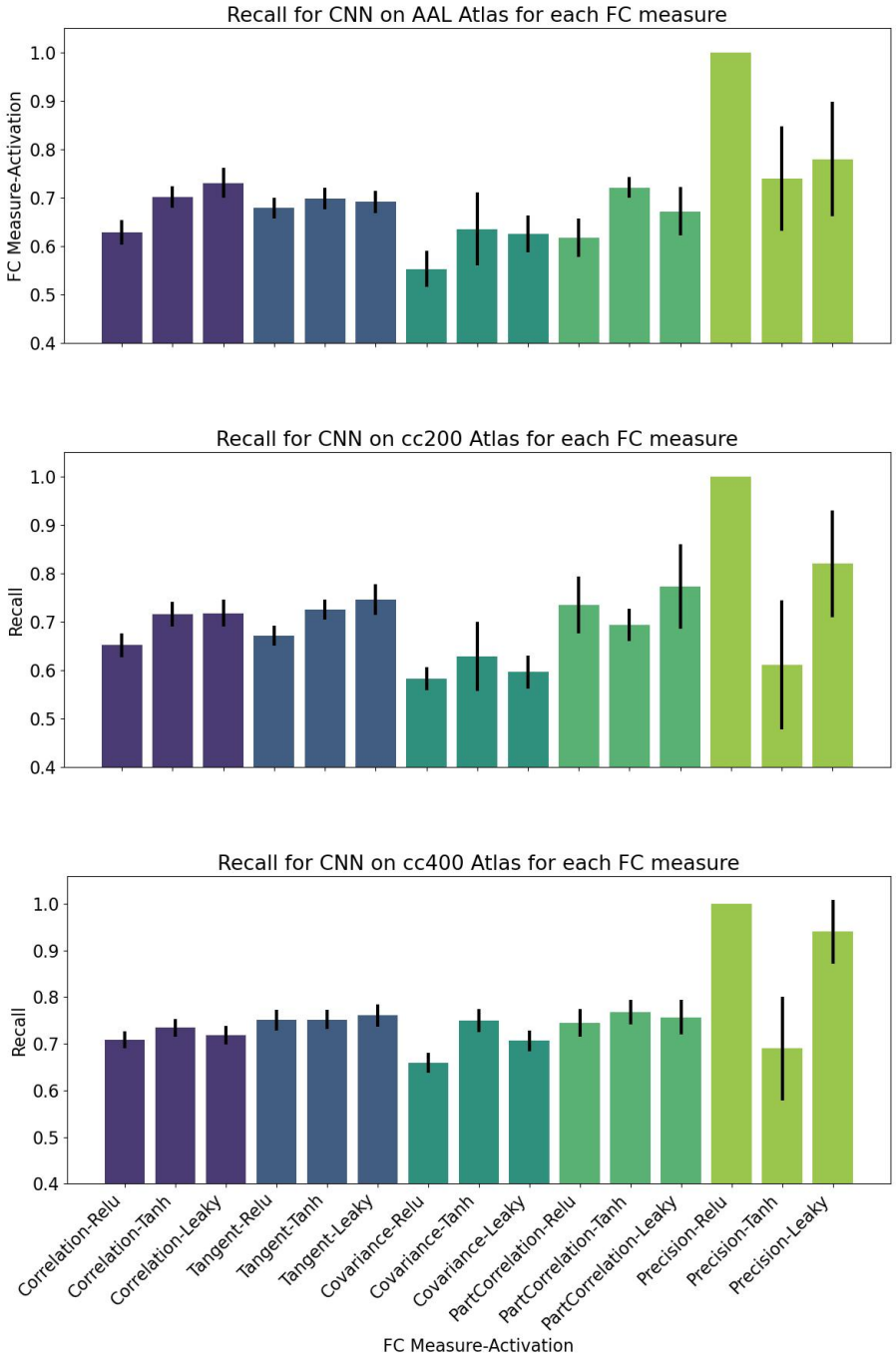

Figure 17: The Recall scores for the CNN model on the AAL, cc200, and cc400 atlases

APPENDIX E: GRAPHS FOR CNN TESTS PRECISION

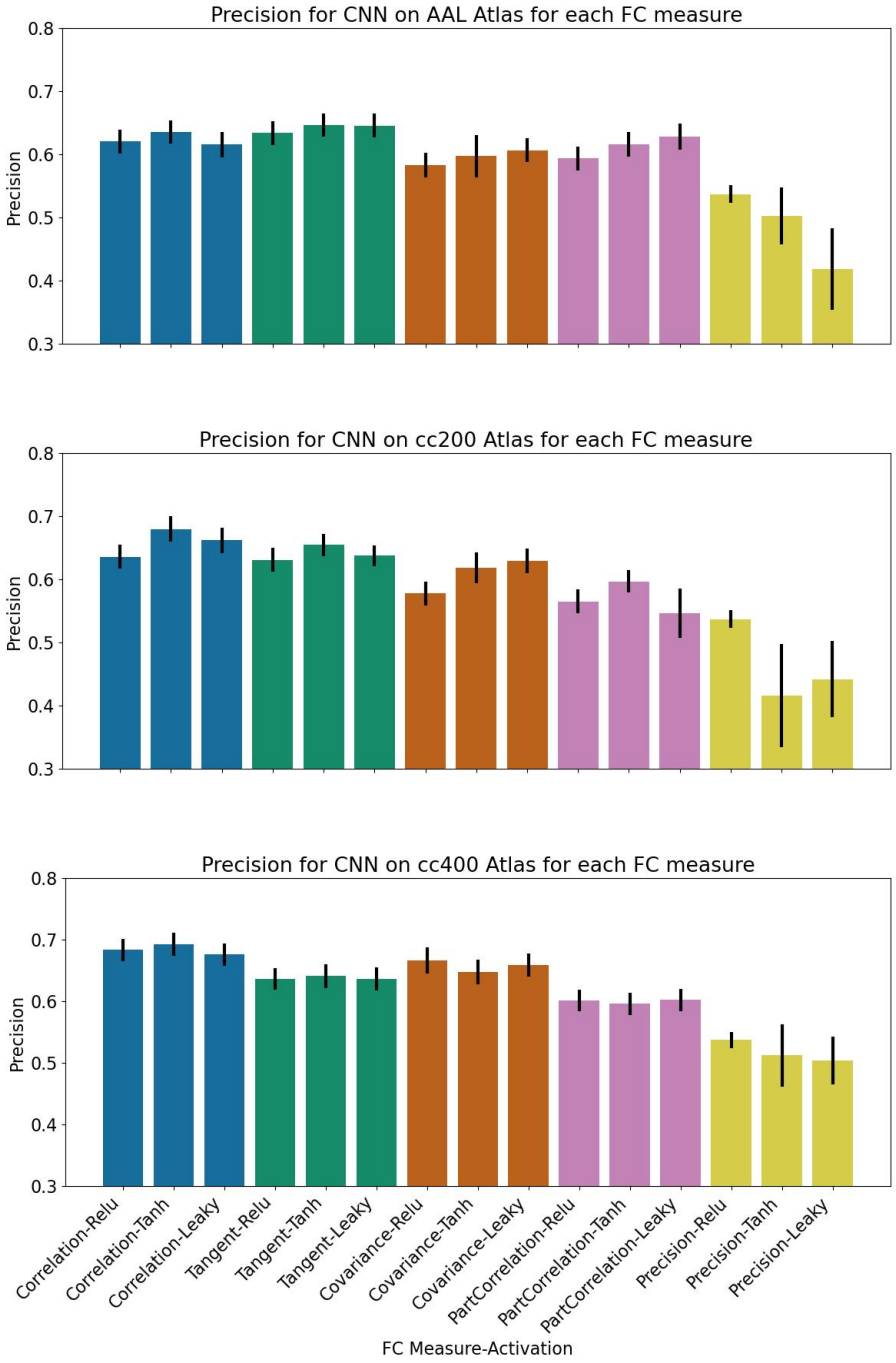

Figure 18: The precision scores for the CNN model on the AAL, cc200, and cc400 atlas

APPENDIX F: COMPLETE SVM TEST TABLES

Table 14: The Accuracy for each test using the Support Vector Machine.

Kernel-FC Measure	AAL	cc200	cc400
Linear-Correlation	0.6548 ± 0.0158	0.6760 ± 0.0140	0.6943 ± 0.0117
RBF-Correlation	0.6516 ± 0.0117	0.6842 ± 0.0134	0.6934 ± 0.0114
Sigmoid-Correlation	0.6590 ± 0.0149	0.6868 ± 0.0137	0.6962 ± 0.0127
Polynomial-Correlation	0.6502 ± 0.0151	0.6941 ± 0.0144	0.6937 ± 0.0122
Linear-Tangent	0.6427 ± 0.0138	0.6675 ± 0.0151	0.6709 ± 0.0148
RBF-Tangent	0.6583 ± 0.0152	0.6673 ± 0.0155	0.6698 ± 0.0151
Sigmoid-Tangent	0.6486 ± 0.0149	0.6675 ± 0.0151	0.6709 ± 0.148
Polynomial-Tangent	0.5681 ± 0.0116	0.5655 ± 0.0097	0.5658 ± 0.0074
Linear-Covariance	0.5899 ± 0.0140	0.6393 ± 0.0148	0.6358 ± 0.0156
RBF-Covariance	0.6583 ± 0.0152	0.6369 ± 0.0147	0.6447 ± 0.0144
Sigmoid-Covariance	0.5373 ± 0.0013	0.5373 ± 0.0013	0.5373 ± 0.0013
Polynomial-Covariance	0.5786 ± 0.0163	0.6225 ± 0.0131	0.6232 ± 0.0176
Linear-Partial Correlation	0.5961 ± 0.0145	0.6184 ± 0.0157	0.6213 ± 0.0153
RBF-Partial Correlation	0.5979 ± 0.0131	0.6181 ± 0.0158	0.6225 ± 0.0140
Sigmoid-Partial Correlation	0.6080 ± 0.0144	0.6207 ± 0.0162	0.6229 ± 0.0160
Polynomial-Partial Correlation	0.5961 ± 0.0127	0.6259 ± 0.0151	0.6211 ± 0.0161
Linear-Precision	0.5940 ± 0.0168	0.6050 ± 0.0139	0.5960 ± 0.0152
RBF-Precision	0.5991 ± 0.0147	0.6101 ± 0.0132	0.6172 ± 0.0163
Sigmoid-Precision	0.5373 ± 0.0013	0.5373 ± 0.0013	0.5373 ± 0.0013
Polynomial-Precision	0.5929 ± 0.0149	0.5749 ± 0.0166	0.5731 ± 0.0143

Table 15: The AUC for each test using the Support Vector Machine.

Kernel-FC Measure	AAL	cc200	cc400
Linear-Correlation	0.648 ± 0.016	0.673 ± 0.014	0.691 ± 0.012
RBF-Correlation	0.647 ± 0.012	0.680 ± 0.014	0.690 ± 0.012
Sigmoid-Correlation	0.653 ± 0.015	0.683 ± 0.014	0.692 ± 0.013
Polynomial-Correlation	0.647 ± 0.015	0.691 ± 0.014	0.691 ± 0.012
Linear-Tangent	0.639 ± 0.014	0.662 ± 0.015	0.664 ± 0.015
RBF-Tangent	0.655 ± 0.015	0.662 ± 0.016	0.663 ± 0.016
Sigmoid-Tangent	0.641 ± 0.015	0.662 ± 0.015	0.664 ± 0.015
Polynomial-Tangent	0.541 ± 0.012	0.536 ± 0.010	0.535 ± 0.008
Linear-Covariance	0.587 ± 0.014	0.638 ± 0.015	0.633 ± 0.016
RBF-Covariance	0.655 ± 0.015	0.633 ± 0.015	0.644 ± 0.015
Sigmoid-Covariance	0.500 ± 0.000	0.500 ± 0.000	0.500 ± 0.000
Polynomial-Covariance	0.572 ± 0.016	0.619 ± 0.013	0.620 ± 0.018
Linear-Partial Correlation	0.592 ± 0.015	0.611 ± 0.016	0.609 ± 0.016
RBF-Partial Correlation	0.593 ± 0.013	0.611 ± 0.016	0.609 ± 0.014
Sigmoid-Partial Correlation	0.602 ± 0.015	0.614 ± 0.016	0.612 ± 0.016
Polynomial-Partial Correlation	0.592 ± 0.013	0.617 ± 0.015	0.608 ± 0.016
Linear-Precision	0.597 ± 0.017	0.605 ± 0.014	0.592 ± 0.015
RBF-Precision	0.597 ± 0.015	0.604 ± 0.013	0.607 ± 0.017
Sigmoid-Precision	0.500 ± 0.000	0.500 ± 0.000	0.500 ± 0.000
Polynomial-Precision	0.592 ± 0.015	0.575 ± 0.016	0.568 ± 0.015

Table 16: The Recall for each test performed with the SVM.

Kernel-FC Measure	AAL	cc200	cc400
Linear-Correlation	0.555 ± 0.019	0.636 ± 0.023	0.645 ± 0.021
RBF-Correlation	0.589 ± 0.019	0.622 ± 0.022	0.639 ± 0.020
Sigmoid-Correlation	0.575 ± 0.018	0.637 ± 0.021	0.643 ± 0.022
Polynomial-Correlation	0.600 ± 0.020	0.648 ± 0.020	0.653 ± 0.020
Linear-Tangent	0.596 ± 0.023	0.593 ± 0.023	0.577 ± 0.025
RBF-Tangent	0.604 ± 0.022	0.592 ± 0.024	0.578 ± 0.027
Sigmoid-Tangent	0.539 ± 0.025	0.593 ± 0.023	0.577 ± 0.025
Polynomial-Tangent	0.182 ± 0.018	0.141 ± 0.018	0.126 ± 0.015
Linear-Covariance	0.553 ± 0.022	0.620 ± 0.023	0.601 ± 0.023
RBF-Covariance	0.604 ± 0.022	0.580 ± 0.024	0.633 ± 0.022
Sigmoid-Covariance	0.000 ± 0.000	0.000 ± 0.001	0.000 ± 0.000
Polynomial-Covariance	0.481 ± 0.025	0.578 ± 0.023	0.581 ± 0.028
Linear-Partial Correlation	0.538 ± 0.022	0.515 ± 0.022	0.447 ± 0.026
RBF-Partial Correlation	0.523 ± 0.019	0.515 ± 0.022	0.432 ± 0.024
Sigmoid-Partial Correlation	0.520 ± 0.023	0.517 ± 0.024	0.464 ± 0.025
Polynomial-Partial Correlation	0.530 ± 0.020	0.492 ± 0.023	0.427 ± 0.025
Linear-Precision	0.632 ± 0.024	0.608 ± 0.019	0.538 ± 0.021
RBF-Precision	0.563 ± 0.022	0.522 ± 0.019	0.473 ± 0.028
Sigmoid-Precision	0.000 ± 0.000	0.000 ± 0.000	0.000 ± 0.000
Polynomial-Precision	0.576 ± 0.024	0.574 ± 0.027	0.506 ± 0.022

Table 17: The Precision score for each test performed with the SVM.

Kernel-FC Measure	AAL	cc200	cc400
Linear-Correlation	0.652 ± 0.022	0.655 ± 0.016	0.679 ± 0.013
RBF-Correlation	0.634 ± 0.014	0.674 ± 0.016	0.681 ± 0.014
Sigmoid-Correlation	0.652 ± 0.020	0.672 ± 0.017	0.683 ± 0.014
Polynomial-Correlation	0.629 ± 0.018	0.680 ± 0.018	0.677 ± 0.015
Linear-Tangent	0.619 ± 0.016	0.658 ± 0.019	0.667 ± 0.018
RBF-Tangent	0.639 ± 0.018	0.658 ± 0.020	0.665 ± 0.018
Sigmoid-Tangent	0.644 ± 0.019	0.658 ± 0.019	0.667 ± 0.018
Polynomial-Tangent	0.612 ± 0.041	0.641 ± 0.045	0.679 ± 0.047
Linear-Covariance	0.560 ± 0.016	0.609 ± 0.016	0.608 ± 0.017
RBF-Covariance	0.639 ± 0.018	0.616 ± 0.018	0.613 ± 0.015
Sigmoid-Covariance	0.000 ± 0.000	0.010 ± 0.020	0.000 ± 0.000
Polynomial-Covariance	0.551 ± 0.020	0.597 ± 0.015	0.596 ± 0.019
Linear-Partial Correlation	0.568 ± 0.018	0.606 ± 0.021	0.629 ± 0.023
RBF-Partial Correlation	0.572 ± 0.016	0.606 ± 0.022	0.636 ± 0.023
Sigmoid-Partial Correlation	0.586 ± 0.018	0.608 ± 0.021	0.626 ± 0.024
Polynomial-Partial Correlation	0.568 ± 0.015	0.625 ± 0.022	0.636 ± 0.026
Linear-Precision	0.554 ± 0.016	0.571 ± 0.015	0.568 ± 0.017
RBF-Precision	0.568 ± 0.016	0.590 ± 0.016	0.610 ± 0.021
Sigmoid-Precision	0.000 ± 0.000	0.000 ± 0.000	0.000 ± 0.000
Polynomial-Precision	0.557 ± 0.015	0.545 ± 0.020	0.541 ± 0.017

APPENDIX G: GRAPHS FOR SVM TEST ACCURACY

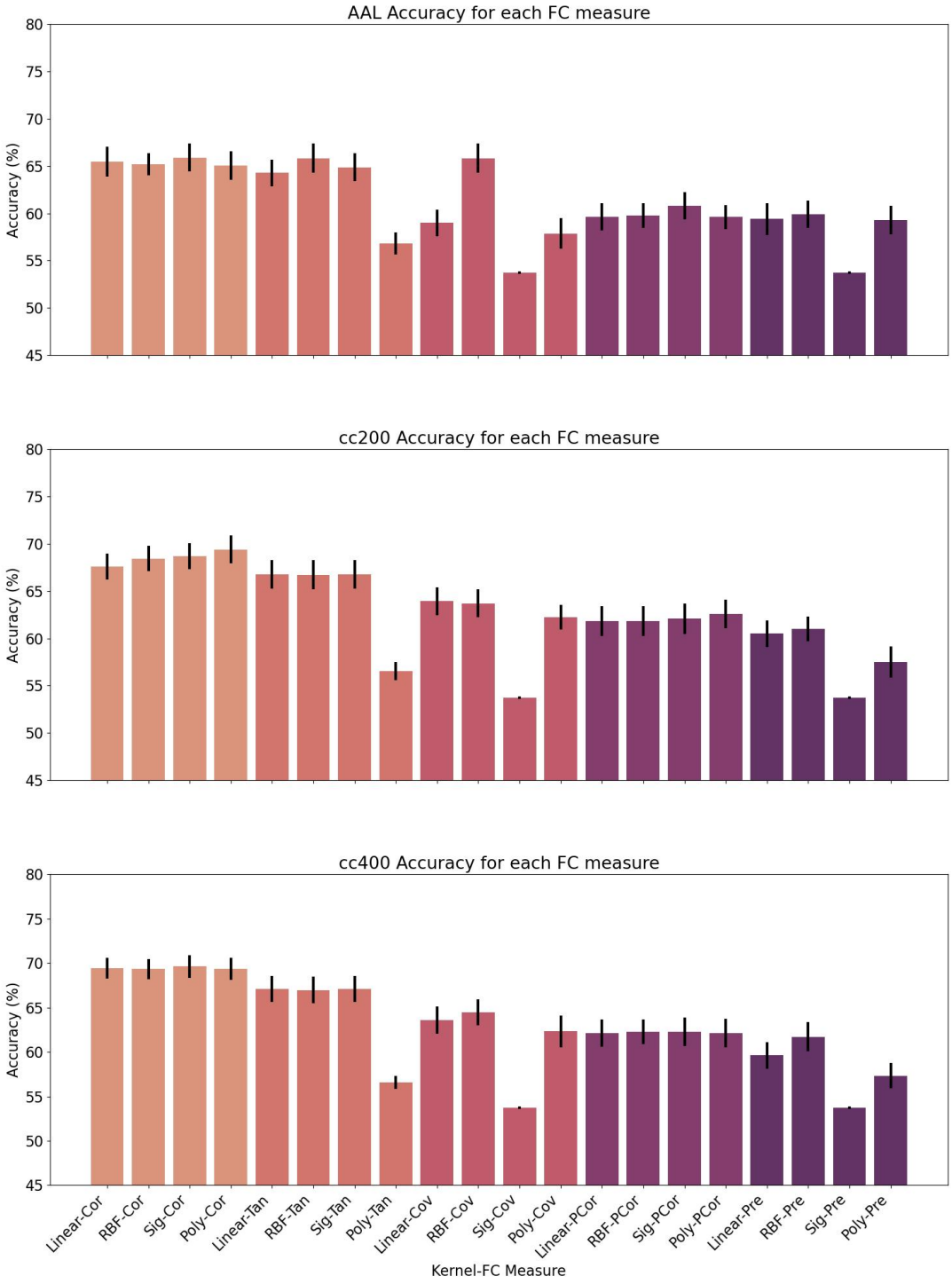

Figure 19: The accuracies for the SVM model on the AAL, cc200, and cc400 atlas

APPENDIX H: GRAPHS FOR SVM TEST AUC

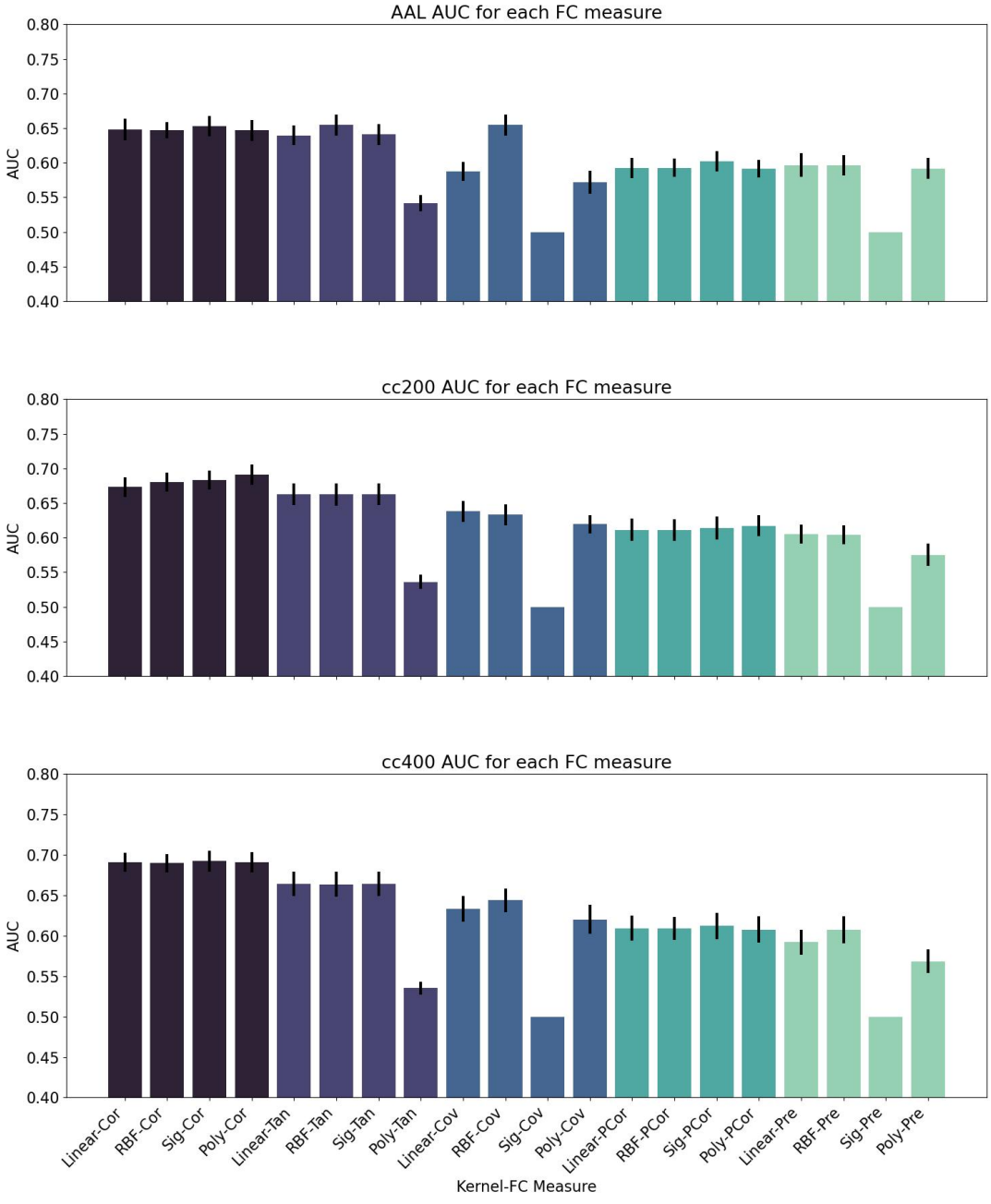

Figure 20: The AUC scores for the SVM model on the AAL, cc200, and cc400 atlas

APPENDIX I: GRAPHS FOR SVM TEST RECALL

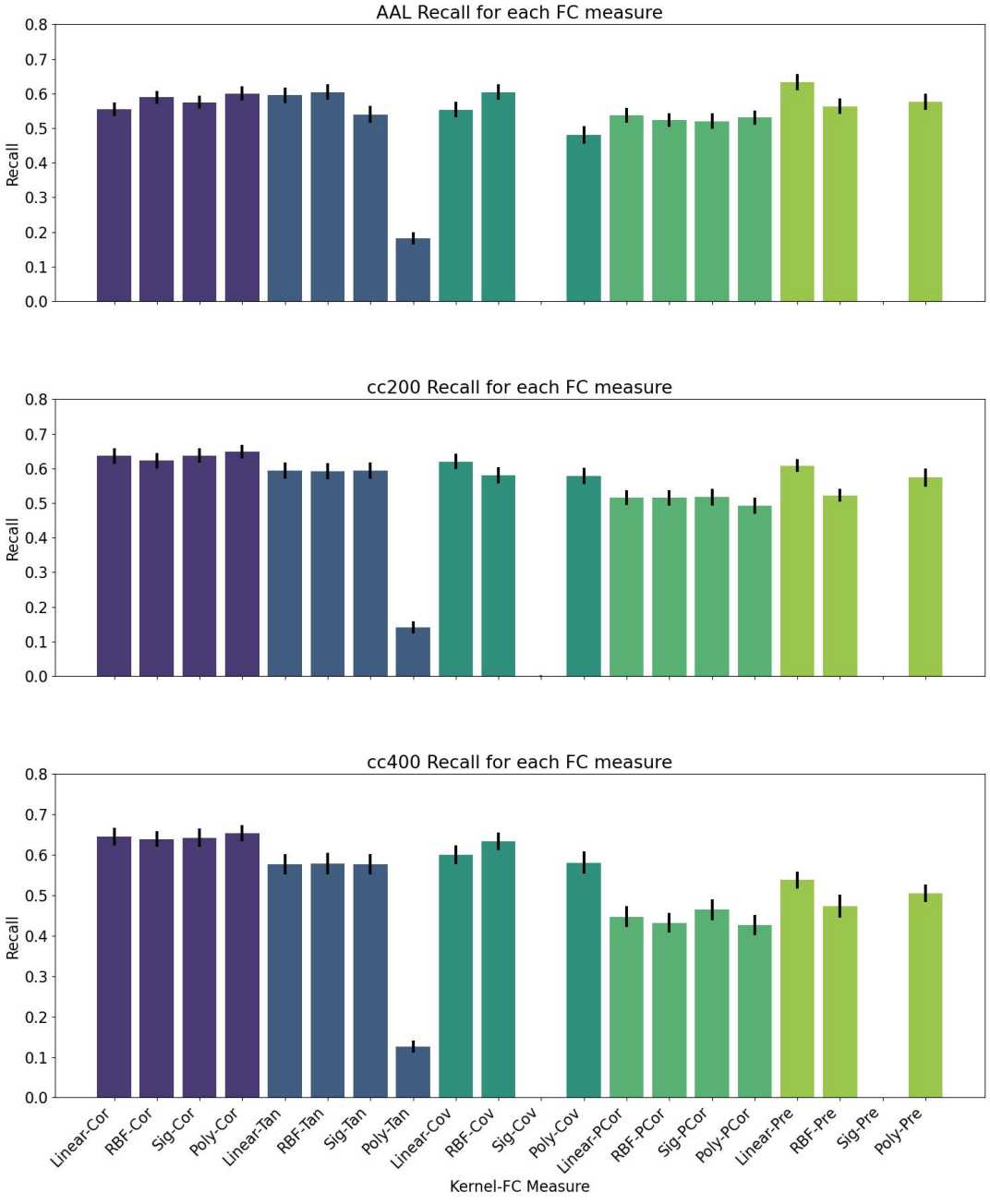

Figure 21: The Recall scores for the SVM model on the AAL, cc200, and cc400 atlas

APPENDIX J: GRAPHS FOR SVM TEST PRECISION

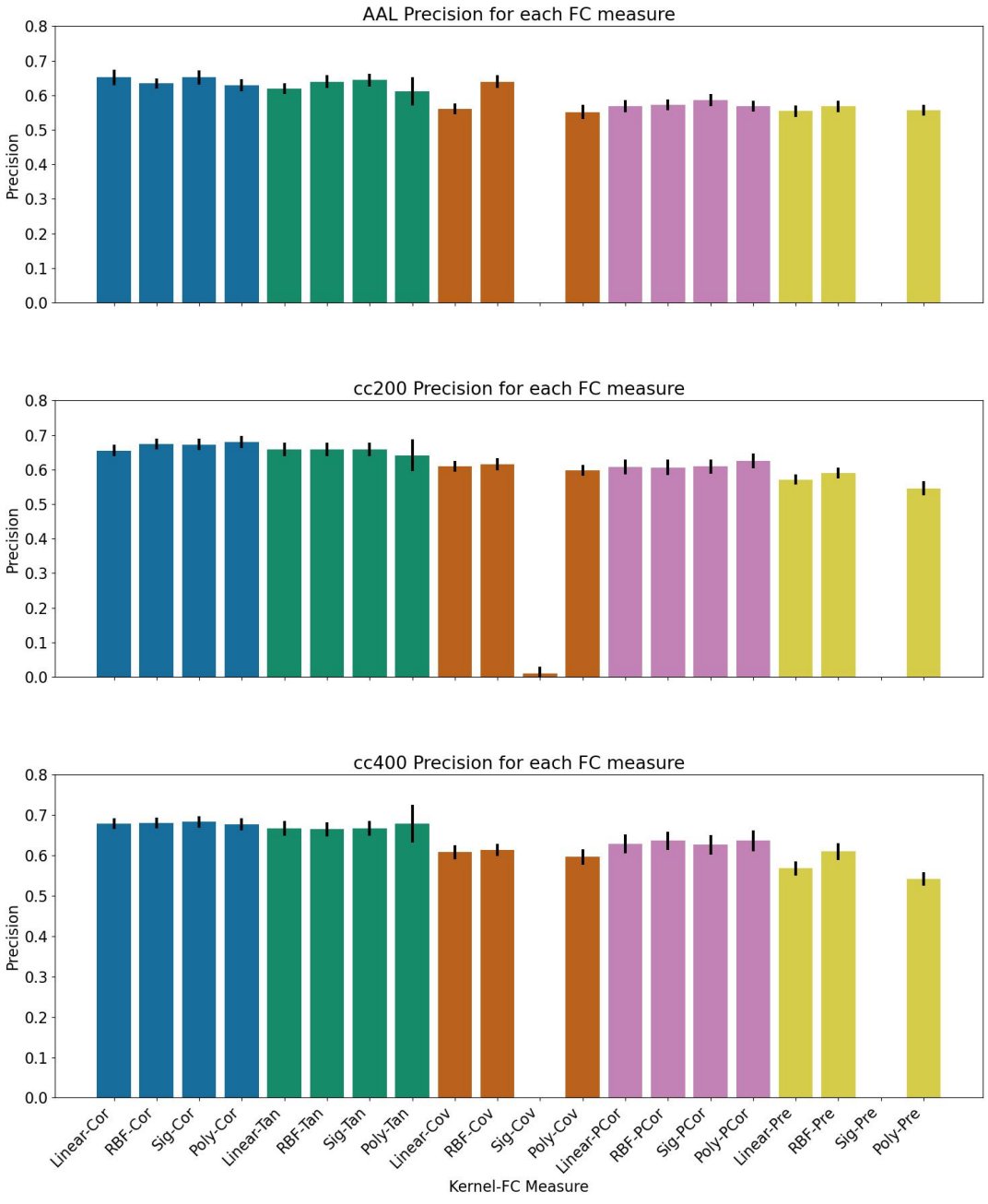

Figure 22: The Precision scores for the SVM model on the AAL, cc200, and cc400 atlas